2.4S.6 Probable Maximum Tsunami Hazards

This subsection examines the Probable Maximum Tsunami (PMT) at the STP 3 & 4 site.

Evaluation of the PMT, as defined by Reference 2.4S.6-1, requires the use of best available scientific information to arrive at a set of scenarios reasonably expected to affect a nuclear power plant site. Reference 2.4S.6-1 recommends a hierarchical hazard assessment for screening exposure to hazards from natural phenomena. The hierarchical screening process is based on a series of stepwise, progressively more refined analyses that evaluate hazards resulting from a tsunami. The hierarchical hazard assessment includes regional screening, site screening, and, if necessary, a detailed PMT hazard assessment.

For this subsection, a tsunami may be characterized as a solitary positive wave, a negative wave coupled with a positive wave (i.e., an N-wave), a series of waves, or any combination of wave types with parameters defined by Table 2.4S.6-1 and Table 2.4S.6-2.

The STP 3 & 4 site is located about 15 mi (24 km) from the South Texas coast (Figure 2.4S.6-1). The site is about 3.2 mi west of the Lower Colorado River, and about 17 river miles, as measured in plan view along the Lower Colorado River, from the South Texas coast. The site grade elevations in the STP 3 & 4 power block area range from 32 ft MSL to 36.6 ft MSL, and all safety-related facilities in the power block are designed to be water tight at or below elevation 40.0 ft MSL as discussed in Subsection 2.4S.10. In addition, the Ultimate Heat Sink (UHS) and Pump House are designed to be watertight below 50 ft MSL (Subsection 2.4S.2.2). Flooding from tsunami events is not expected to affect the safety functions of the plant as discussed below.

2.4S.6.1 Probable Maximum Tsunami

Tsunamis are gravity waves generated by large underwater disturbances. Reference 2.4S.6-1, Reference 2.4S.6-2, and Reference 2.4S.6-3 identify several types of tsunamigenic source mechanisms, including seismic events, volcanic events, submarine mass failures (SMFs), subaerial landslides, and impact of projectiles. With respect to a tsunami hazard assessment for the STP 3 & 4 project site, three primary forcing mechanisms are included in the analysis: seismic events, volcanic events, and SMFs (Reference 2.4S.6-1).

The tsunami hazard on the Gulf coast is summarized in Reference 2.4S.6-3. With respect to seismic events, Reference 2.4S.6-3 states that “tsunamis generated by earthquakes do not appear to impact the Gulf of Mexico coast.” Further, simulations of postulated “worst-case” far-field (i.e., tsunami sources originating from over 1000 km away) seismic events with potential to affect the US Gulf coast indicate a maximum wave height of about 0.15 m at the South Texas coast (Reference 2.4S.6-4). With respect to volcanic events, the largest conjectured event with potential to affect the US Atlantic and Gulf coasts has been postulated to be a tsunami from the eruption and collapse of the Cumbre Vieja volcano on the island of La Palma in the Canary Islands

(Reference 2.4S.6-5). However, Reference 2.4S.6-3 indicates that this event is unlikely to affect the Gulf coast.

With respect to SMFs, Reference 2.4S.6-3 identifies several large SMF scars in carbonate, salt, and canyon to deep-sea provinces in the Gulf of Mexico. Many scars in these provinces correspond with relic events throughout the Quaternary (i.e., from 2.6 million to about 7500 years before the present, or yr BP). Multiple events have been identified for each scar. Notably, the geomorphology of SMFs in the Gulf of Mexico has been shown to be coupled with changes in sea level (Reference 2.4S.6-6 and Reference 2.4S.6-7). Reference 2.4S.6-6 documents sea-level changes over the last 140,000 years, with the last lowstand of 120 m below present sea level occurring less than 20,000 years ago.

With respect to near-field tsunami hazards at STP 3 & 4 (i.e., tsunamigenic sources within 124 mi or 200 km), the most prominent SMF scar is the East Breaks slump. The East Breaks slump is located approximately 88.2 mi (142 km) to the southeast of STP 3 & 4. Characterization and analysis of the East Breaks slump are discussed in detail in Subsection 2.4S.6.4.

Based on the hierarchical hazard assessment, the PMT for the STP 3 & 4 site is conjectured to occur from an SMF similar to the East Breaks slump. However, as the interpretation of a single wave height from a slump scar may not be sufficient to bound the PMT flood risks on STP 3 & 4 due to the uncertainties inherent in the assessment, a range of potential conditions were simulated at the East Breaks slump location. Simulations were performed using a hydrodynamic code known as the Method of Splitting Tsunami (MOST) (References 2.4S.6- 8 and 2.4S.6-9). These simulations were intended to bracket any near-field tsunami hazard from a SMF in the Gulf of Mexico.

Initial conditions of a negative wave (i.e., a wave caused by the drawdown of the water surface due to a sliding mass) were based on curve fits of sliding block experiments of Reference 2.4S.6-10 and Reference 2.4S.6-11. These initial conditions were subsequently scaled into a three-dimensional dipole wave (i.e., a negative wave and positive wave with unequal intensities) based on relationships presented in References 2.4S.6-12, 2.4S.6-13, and 2.4S.6-14.

The SMF scenarios postulated include initial wave deformation areas (i.e., areas differing from MSL) ranging from 410 km^2 to 9932 km^2 (158 mi^2 to 3835 mi^2, respectively). Four scenarios were modeled as candidate PMT events. The simulation results indicate that all candidate PMT events were rapidly diffused by the continental shelf offshore of the South Texas coast, with nearly all remaining wave energy being reflected by the barrier islands. For negative wave elevations ranging from -7 m (23.0 ft) to -140 m (459.3 ft) and positive wave elevations ranging from 3 m (9.84 ft) to 60 m (197 ft), maximum predicted runup from the simulations did not exceed 2 m (6.6 ft) above MSL. Maximum flow depth from these simulations did not exceed 3.25 m (10.7 ft).

The evaluation of the maximum flood level for a PMT event also included an analysis of the 10% exceedance of the astronomical high tide and long-term sea level rise. As regulatory criteria for these components are only available for the Probable Maximum Storm Surge (PMSS), the criteria for the PMSS in Regulatory Guide 1.59 (1977) (Reference 2.4S.6-15) were adopted for the PMT analysis. Based on tide gage data for NOS Station #8772440, which is located in Freeport, Texas, the 10% exceedance of the astronomical high tide was estimated to be 3.54 ft (1.08 m) MSL (Reference 2.4S.6-16). The long-term sea level rise for this station was estimated by NOAA to be 0.171 in (4.35 mm) per year or 1.43 ft (0.44 m) per century (Reference 2.4S.6-17). The peak flood level due to a PMT event is therefore estimated to be of the order of 11.5 ft (3.52 m) MSL within the next century (i.e., 6.56 ft tsunami runup + 3.54 ft 10% exceedance of the astronomical high tide + 1.43 ft sea-level rise = 11.5 ft MSL).

A tsunami runup of 11.5 ft MSL is below the design basis flood level of 40.0 ft MSL that is postulated from a Main Cooling Reservoir (MCR) breach event (Subsection 2.4S.4). PMT is therefore not the controlling event for the design basis flood determination for STP 3 & 4 safety-related structures.

2.4S.6.2 Historical Tsunami Record

Information and data on tsunami-generating earthquakes and runup events are included in the National Geophysical Data Center (NGDC) hazards database (Reference 2.4S.6-18). The NGDC database contains information on source events and runup elevations for worldwide tsunamis from about 2000 BC to the present (Reference 2.4S.6-1). Each event in the NGDC database has a validity rating ranging from 0 to 4, with 0 for erroneous events, 1 for very doubtful events, 2 for questionable events, 3 for probable events, and 4 for definite events. Similarly, each event includes a cause code identifying the forcing mechanism (e.g., earthquake, volcano, landslide, or any combination thereof).

With respect to published literature, the publication titled “Caribbean Tsunamis: A 500-Year History from 1498-1998,” is a compendium of data and anecdotal material on tsunamis reported in the Caribbean from 1498 to 1997 (Reference 2.4S.6-19). Reference 2.4S.6-20 includes source events and runup elevations for the Caribbean Sea and Eastern United States from 1668 to 1998, respectively. The USGS has published a fact sheet showing locations of plate boundaries in the Caribbean and tsunami-generating earthquakes from 1530 to 1991 (Reference 2.4S.6-21). The map is shown in Figure 2.4S.6-2. Additionally, NOAA’s Center for Tsunami Research, in conjunction with the Pacific Marine Environmental Laboratory, publishes information and analyses on tsunami sources and tsunami events (Reference 2.4S.6-22).

Three historical tsunami runup events have been documented for the State of Texas, USA, in the NGDC database and in published literature. The first documented tsunami event for the Texas coast occurred on October 24, 1918. This tsunami was reported to be an aftershock of the M_W=7.5 October 11, 1918, earthquake near Puerto Rico (Reference 2.4S.6-23, p. 73). The epicenter of the earthquake was reported at 18.5º N and 67.5º W (Reference 2.4S.6-19, p. 201), which is approximately nine miles northwest of Puerto Rico and located in the Mona Rift. As described in Reference 2.4S.6-19 (p. 201), this earthquake was “considered a terrific aftershock of the October

11 event...[with] a small wave [being] recorded at the Galveston, Texas, tide gage." This event has a validity rating of four. The magnitude of tsunami runup was not reported.

The second documented tsunami event for the Texas coast occurred on May 2, 1922. The epicenter of the earthquake associated with this event was reported at 18.4º N and 64.9º W (Reference 2.4S.6-19, p. 201). Reference 2.4S.6-19 (p. 201) stated that "a wave with an amplitude of 64 cm was reported on a tide gage at Galveston. A train of three waves with a 45-minute period was followed in 8 hours by a 28-cm wave in a similar train of smaller waves. Parker [Reference 2.4S.6-24] associated it with an earthquake felt 4 hours earlier at Vieques, Puerto Rico." However, according to Campbell [Reference 2.4S.6-25, p. 56], the shock had a duration of only two seconds. Therefore, the earthquake is unlikely to have been the tsunamigenic source. The validity rating of this event in the NGDC database is a two (i.e., a questionable event). No runups were documented along the Gulf coast for the primary shock of the 1922 earthquake. The surge was presumed to have been locally amplified by the inland position of the tidal gage (Reference 2.4S.6-24, p. 30). The magnitude of the 1922 earthquake or the aftershock has not been estimated.

The third documented tsunami event for the Texas coast occurred on March 27, 1964. The event was recorded on a tide gage in Freeport, Texas (Reference 2.4S.6-26). While the validity of this event was a four, estimates of the wave height vary considerably between eyewitness accounts and tide gage data. Reference 2.4S.6-26 (p. 261) notes that "in several reports from eyewitnesses in the coastal regions of Louisiana and Texas, waves up to 6 feet (2 meters) in height were observed." However, Reference 2.4S.6-26 (p. 261) reports that the "maximum height of the recorded seiche at 0400 GMT is about seven inches (18 cm)," and that the "true wave height may have been several feet ([i.e.,] about a meter)." This event coincided with the 1964 Alaska (M_w=9.2) earthquake located between the Aleutian Trench and the Aleutian Volcanic Arc (Reference 2.4S.6-27). Additional analyses of tide gage records from the 1964 event report the maximum measured height of the low-frequency waves along the Texas coast from the Alaska earthquake ranged from 0.22 to 0.84 feet (Reference 2.4S.6-28, p. 26).

2.4S.6.3 Source Generator Characteristics

Tsunamigenic source characteristics with potential to affect the US Atlantic and Gulf coasts are summarized in Reference 2.4S.6-3, several databases, and published literature as discussed in the following subsections.

2.4S.6.3.1 Seismic tsunamis

In comparison to tsunami runup events that have been documented in the Caribbean (Reference 2.4S.6-29), the Texas coast has had relatively few runup events. For example, as noted previously, Reference 2.4S.6-3 (p. ii) stated that "tsunamis generated by earthquakes do not appear to impact the Gulf of Mexico coast." However, tsunamigenic earthquake sources that may affect the Gulf of Mexico are discussed in Reference 2.4S.6-3 (pp. 105-112). As stated in Reference 2.4S.6-3 (p. 105):

> "Earthquake-generated tsunamis generally originate by the sudden vertical movement of a large area of the seafloor during an earthquake. Such movement is generated by reverse faulting, most often in subduction zones. The Gulf of Mexico basin is devoid of subduction zones or potential sources of large reverse faults. However, the Caribbean basin contains two convergence zones whose rupture may affect the Gulf of Mexico, the North Panama Deformation Belt and the Northern South America Convergent Zone."

As stated in Reference 2.4S.6-3, source areas with potential for tsunamigenesis affecting the US Gulf Coast include the North Panama Deformation Belt and the Northern South American Convergent Zone (Table 2.4S.6-3). With respect to the North Panama Deformation Belt, Reference 2.4S.6-3 stated that:

> "the largest segment of the North Panama Deformation Belt is oriented between 60°-77°. The 1882 Panama earthquake appears to have ruptured at least 3/4 of the available length of the convergence zone, and was estimated to have a magnitude of 8. While there was significant tsunami damage locally, there were no reports from the Gulf of Mexico of a tsunami from this earthquake. The low convergent rate (7-11 mm/yr) across the North Panama Deformation Belt supports long recurrence interval for large earthquakes."

The Harvard Centroid-Moment-Tensor (CMT) catalog was searched for potential seismogenic earthquakes in the two source regions of Table 2.4S.6-3 (Reference 2.4S.6-30). The following criteria were used for searching the CMT catalog within the North Panama Deformation Belt: a date range of 01/01/1976 (i.e., the start of the database) through 11/04/2008; latitude from 9° N to 12° N; longitude from 83° W to 77° W; depth from 0 to 1000 km; and moment magnitude (M_w) range from 6.5 to 10. The selection of a lower bound of M_w=6.5 is based on criteria from Reference 2.4S.6-2 (p. 23) for a threshold moment magnitude of tsunamigenesis from earthquakes. One record was identified in the CMT catalog with these criteria. On 04/22/1991, a M_w=7.6 earthquake occurred at depth of 15 km and at a latitude of 10.10° N and a longitude of 82.77° W, located about 20 mi. (32 km) offshore of the town of Limon, Costa Rica. Source parameters for the earthquake were documented as a strike of 103 degrees, a dip of 25 degrees, and a rake of 58 degrees. Source parameters for earthquakes in the North Panama Deformation Belt with moment magnitudes below 6.5 are discussed in Reference 2.4S.6-3. With respect to the far-field tsunami hazard on the South Texas coast, these additional sources are not reasonably expected to exceed the tsunamigenic potential of scenarios simulated by Reference 2.4S.6-3 and Reference 2.4S.6-4.

The following criteria were used for searching the CMT catalog within the Northern South American Convergent Zone: a date range of 1/1/1976 to 11/04/2008; latitude from 11.5° N to 14° N; longitude from 77° W to 64° W; depth from 0 to 1000 km; and moment magnitude range from 6.5 to 10. No records were identified in the CMT catalog with these criteria. By broadening the criteria to include earthquakes from $0<M_w<10$, two records were returned. The moment magnitude of the two earthquakes was 5.1. Moment magnitudes of 5.1 are below the generally accepted threshold required for seismic tsunamigenesis as defined by Reference 2.4S.6-2 (p. 23).

Therefore, the assessment of far-field tsunami hazards in this region was based on tsunami simulations in References 2.4S.6-4 and 2.4S.6-3. Reference 2.4S.6-4 performed tsunami simulations of seismic-borne tsunamis from postulated "worst-case" events using a two-dimensional depth-integrated hydrodynamic model described in Reference 2.4S.6-31. The following cases were used in the assessment (Reference 2.4S.6-4, p. 305):

1. M_w=9.0 at 66° W and 18° N (Puerto Rico trench);

2. M_w=8.2 at 85° W and 21° N (Caribbean Sea);

3. M_w=9.0 at 66° W and 12° N; and

4. M_w=8.2 at 95° W and 20° N (near Veracruz, Mexico).

The source location of Case 3 at 66° W and 12° N is cited in Reference 2.4S.6-4 (p. 305) as the North Panama Deformation Belt, but the location corresponding to 66° W and 12° N is the South Caribbean Deformed Belt (Reference 2.4S.6-3, p. 110).

Source parameters for the model cases in Reference 2.4S.6-4 were based on the formulae of Reference 2.4S.6-32. For example, source parameters for the Veracruz scenario (Reference 2.4S.6-4, p. 305) are provided in Table 2.4S.6-4. Reference 2.4S.6-4 (p. 305) stated that the model sources were aligned with local strike.

Reference 2.4S.6-4 (p. 311) concluded that "sources outside the Gulf are not expected to create a tsunami threatening to the Gulf coast." Reference 2.4S.6-4 attributed this result primarily due to friction losses as the waves travel through the Straits of Florida and throughout islands in the Caribbean. Tsunami simulations in Reference 2.4S.6-3 complemented earlier work by Reference 2.4S.6-4, with Reference 2.4S.6-3 (p. 117) stating that:

> "in general, these results are consistent with the findings of Knight (2006) [Reference 2.4S.6-4], where the far-field tsunamis generated from earthquakes located beneath the Caribbean Sea are higher along the Gulf coast than the Atlantic coast because of dissipation through the Greater Antilles islands. Conversely, tsunamis generated from earthquakes north of the Greater Antilles are higher along the Atlantic coast than the Gulf coast."

Reference 2.4S.6-4 (p. 311) stated that one reason for this conclusion was that "the Atlantic and Gulf coasts are nearly independent since the hydrodynamic connection between basins is through the narrow Straits of Florida and through the Caribbean, where bottom friction losses appear to be large."

Additionally, the largest deepwater wave from the Reference 2.4S.6-3 simulations was produced from the north Venezuela subduction zone. The maximum wave height from the north Venezuela subduction zone from a buoy at a depth of 250-m offshore of New Orleans, Louisiana, was estimated to be 6 cm (Reference 2.4S.6-3, p. 130, Figure 7-4e, "Station 1").

While tsunamigenic earthquakes within the Gulf of Mexico have not been recorded, Reference 2.4S.6-4 included a tsunami simulation assuming a magnitude M_w=8.2 earthquake offshore of Veracruz, Mexico. The resulting wave amplitude at the South Texas coast was about 0.35 m. Intraplate earthquakes are less common than earthquakes occurring on faults near plate boundaries, but several earthquakes in the past three decades had epicenters within the Mississippi Canyon and Fan province (Reference 2.4S.6-3). In recent time, the most severe earthquake in this region occurred on September 10, 2006. The moment magnitude was recorded as 5.8. The second largest earthquake in this region occurred on February 10, 2006 with a moment magnitude of 5.2. The United States Geological Survey (USGS) concluded that earthquakes of this magnitude are unlikely to produce any destructive tsunami (Reference 2.4S.6-33).

2.4S.6.3.2 Seismic seiches

The only documented event of a seismic seiche on the Texas coast is from the 1964 Alaska earthquake. Reference 2.4S.6-28 indicated that the horizontal acceleration associated with seismic surface waves from the Alaska shock appears to have varied markedly within North America. The amplitude of horizontal acceleration was especially large along the Gulf coast. Reference 2.4S.6-28 (p. 27) further stated that "thick deposits of sediments of low rigidity along the Gulf coast, for example, are capable of amplifying the horizontal acceleration of surface waves to a considerable extent; this accounts for the concentration of seiches that occurred along the Gulf coast."

While the M_w=9.5 magnitude 1960 earthquake in Chile might also have been expected to have caused seiches along the Texas coast, tide gages along the Gulf coast did not record any event. The M_w=7.8 New Madrid earthquake that occurred on February 7, 1812 (Reference 2.4S.6-34), which is the largest earthquake recorded in the contiguous United States, produced significant seiches in the Mississippi River and in waterways along the Texas state boundary (Reference 2.4S.6-20, p. 124). However, no records exist to indicate that the 1812 New Madrid earthquake directly affected the South Texas coast or the Lower Colorado River near STP 3 & 4.

2.4S.6.3.3 Volcanism-based tsunamis

Reference 2.4S.6-3 did not cite a tsunami hazard to the Gulf coast from volcanism. For example, Reference 2.4S.6-3 stated that "far-field landslides, such as in the Canary Islands, are not expected to cause a devastating tsunami along the U.S. Atlantic coast." Previous studies have conjectured that the eruption and collapse of the Cumbre Vieja volcano on the island of La Palma in the Canary Islands could potentially affect the coast of Florida, USA, with a 25-m wave (Reference 2.4S.6-5). A recent assessment of Reference 2.4S.6-5 was discussed in Reference 2.4S.6-3 (p. 57):

> "as envisioned by Ward and Day (2001) [Reference 2.4S.6-5], a flank collapse of the volcano may drop a rock volume of up to 500 km^3 into the surrounding ocean. The ensuing submarine slide, which was assumed to propagate at a speed of 100 m/s, will generate a strong tsunami with amplitudes of 25 m in Florida. In addition, [Ward and Day, 2001] claimed that the collapse of Cumbre

> Vieja is imminent. In our opinion, the danger to the U.S. Atlantic coast from the possible collapse of Cumbre Vieja is exaggerated. Mader (2001) [Reference 2.4S.6-35] pointed out that Ward and Day's (2001) assumption of linear propagation of shallow water waves is incorrect, because it only describes the geometrical spreading of the wave and neglects dispersion effects. A more rigorous hydrodynamic modeling by Gisler et al. (2006) [Reference 2.4S.6-36], confirms Mader's criticism. Their simulations show significant wave dispersion and predict amplitude decay proportional to r-1 for a 3-dimensional model and r-1.85 for a 2- D model (r is distance). [Reference 2.4S.6-36] predicted [a] wave amplitude for Florida is between 1 [and] 77 cm. [Reference 2.4S.6-36 used] slightly smaller volume, 375 km^3, than Ward and Day (2001), but a much higher slide speed, that is much closer to the phase speed for tsunamis in the deep ocean (4,000 m of water)."

Further research on the La Palma event indicated that the distribution of slide blocks on the ocean bottom suggests that the collapse of Cumbre Vieja may not have been the result of a single catastrophic event, but the result of several smaller events. A recent report on potential tsunami threats to the United Kingdom concluded that "studies of the offshore turbidities [i.e., poorly sorted sediment that is deposited from a density flow of mixed water and sediment] created by landslides from the flanks of the Canary Islands suggest that these result from multiple landslides spread over periods of several days" and are therefore "likely to create tsunamis of only local concern" (Reference 2.4S.6-37, p. 23 and p. 30, respectively).

As no tsunamis have been documented in the Gulf of Mexico as a result of recent volcanic eruptions or associated mass wasting events (i.e., gravity-driven mass movement of soil, regolith, or rock moving downslope), this mechanism is not considered further as a potential source of tsunamis along the South Texas Coast.

2.4S.6.3.4 Submarine slump tsunamis

Reference 2.4S.6-3 (p. 35) cites four credible SMF source areas in the Gulf of Mexico: the Florida Escarpment, Campeche Escarpment, Northwest Gulf of Mexico, and the Mississippi Canyon (Figure 2.4S.6-3). These four SMF source areas are located in three geologic provinces: a carbonate province, a salt province, and a canyon to deep-sea fan province.

The postulated SMF sources in the carbonate province are located offshore of West Florida and in the Campeche Escarpments north of the Yucatan Peninsula (Reference 2.4S.6-3). The largest scar in this region is along the central part of the West Florida Slope and is estimated as 120 km long, 30 km wide, with a total volume of material removed of about 1,000 km^3. However, formation of the scar was believed to have occurred as a result of multiple events. Most of the sediment was estimated to have been removed before the middle of the Miocene [c. 11.6 million years ago]. Reference 2.4S.6-3 (p. 28) stated the following:

> "During the Mesozoic, an extensive reef system developed around much of the margin of the Gulf of Mexico Basin by the vertical growth of reefs and carbonate shelf edge banks. This reef system is exposed along the Florida Escarpment

> and the Campeche Escarpment that fringe the eastern and southern margins of this basin. These escarpments stand as much as 1,500 m above the abyssal plain floor, and have average gradients that commonly exceed 20° and locally are vertical. Reef growth ended during the Middle Cretaceous, and subsequently the platform edges have been sculpted and steepened by a variety of erosional processes."

The salt province is located in the northwestern Gulf of Mexico. Reference 2.4S.6-3 (p. 32) stated that Geologic Long-Range Inclined Asdic (GLORIA) imagery identified 37 SMFs in the salt province and along the base of the Sigsbee Escarpment. The largest of these landslides is the East Breaks slump, which is discussed in additional detail below. With respect to the morphology of the salt province, Reference 2.4S.6-3 (pp. 27-28) stated the following:

> "Salt deposited in the late Jurassic Gulf of Mexico basin, the Louann salt, originally underlay large parts of Louisiana, southern Texas, and the area offshore of Mexico in the Bay of Campeche. As sediment eroded from the North American continent was deposited on this salt sheet throughout the Mesozoic and Cenozoic, the increased load caused the salt to flow with it migrating southward from the source area into the northern Gulf of Mexico. Presently the Louann salt underlies large parts of the northern Gulf of Mexico continental shelf and continental slope. South of Louisiana and Texas, the Sigsbee Escarpment is a pronounced cliff that marks the seaward limit of the shallowest salt tongue. As the salt is loaded, it flows both seaward and also upward through the overlying sediment column as cylindrical salt domes. The morphology of the salt sheet varies considerably across the margin. Salt domes are most common under the continental shelf, and most of the original salt sheet between individual domes in this region has been removed in response to the sediment loading, and migrated farther seaward."

Other SMFs identified in the salt province have areas that are an order of magnitude lower than the East Breaks slump (Reference 2.4S.6-3), and are not further considered.

Three canyon to deep-sea fan systems were formed during the Pliocene and Pleistocene: the Mississippi, Eastern Mississippi, and Bryant systems (Figure 2.4S.6-3). The Mississippi system is the largest of the three systems, though Reference 2.4S.6-3 states that the resumption of hemipelagic sedimentation at the head of the Mississippi Canyon by 7500 yr BP indicates that the largest of the landslide complexes ceased being active by the middle of the Holocene. The largest SMF in the complex covers approximately 23,000 km^2 and reaches 100 m in thickness, with a volume estimated to be about 1,750 km^3. GLORIA sidescan sonar data suggests that this feature consists of at least two separate events (Reference 2.4S.6-3).

The Eastern Mississippi and Bryan Canyon systems are smaller than the Mississippi Canyon system. The Eastern Mississippi system has a deposit that is "approximately 154 km long, as much as 22 km wide, and covers an area of 2,410 km^2" (Reference

2.4S.6-3, p. 34). With respect to the Bryant system, Reference 2.4S.6-3 (pp. 33-34) states that

> "The Bryant Canyon system was immediately downslope of a shelf edge delta system, and failure of this system has been proposed as the explanation for thick chaotic deposits in mini basins along the path of this canyon system Debris from the failure of the shelf edge delta was transported down the Bryant Canyon system, but these landslide deposits predate and are buried by the smaller landslides off the mini-basin walls."

2.4S.6.4 Tsunami Analysis

Tsunami modeling was conducted for a tsunami originating at the location of the East Breaks slump near the South Texas coast. For all scenarios, the tsunamigenic source was a SMF. As with Reference 2.4S.6-12 and Reference 2.4S.6-13, a series of scaled dipolar initial conditions were used for bracketing a conservative range of initial wave heights. Hydrodynamic simulations were modeled using a series of codes known as the Method of Splitting Tsunami (MOST) (References 2.4S.6-8). For all model simulations, maximum runup along the South Texas coast did not exceed 2 m (6.56 ft) above Mea Sea Level (MSL).

The following paragraphs discuss the geologic setting of the East Break slump, followed by discussion of hydrodynamic simulations with MOST.

The East Breaks slump is located approximately 88.2 mi (142 km) to the southeast of STP 3 & 4 (Figure 2.4S.6-4). The coordinates of the slump are approximately 27.57° N and 95.64° W. The slump is comprised of an eastern lobe and a western lobe. Reference 2.4S.6-38 (p. 2) stated that "the western and eastern lobes are thought to have formed by two different processes, and actually at two different, but relatively close, time periods. The western lobe formed as slump and debris deposits traveled downslope. The eastern lobe is more consistent with turbidity flow currents in the upper parts of the slide and leveed channels in the middle and lower portions of the slide." Further, Reference 2.4S.6-38 (p. 3) stated that "the eastern lobe appears more channelized and consists of density flow-type fill with few large slump and intact blocks. The western lobe, therefore, carried the bulk of the failed material and the energy level of the failure was much greater." As the eastern lobe was unlikely to have influenced tsunamigenesis, only the western lobe was used for the simulations.

The age of the East Breaks slump is not precisely known. Reference 2.4S.6-39 (p. 366) stated that the most recent mass wasting event responsible for the formation of the western lobe occurred about 16,000 yr BP, and after the formation of the bulk of the eastern lobe. Reference 2.4S.6-7 stated that "the East Breaks Slide is a site of [sea level] lowstand instability, and seismic [reflection] data shows repeated slope failure in this area. During late Quaternary lowstands of sea level, large deltas built up along the Texas-Louisiana shelf margin, and the present continental shelf [became] exposed as a subaerial coastal plain." Reference 2.4S.6-7 also stated that "it is clear that most sliding on the Texas-Louisiana slope occurred during the late Pleistocene [c. 10,000 - 29,000 years BP] lowstands of sea level when sedimentation rates on the upper slope were high."

With respect to stability, Reference 2.4S.6-3 notes that information on the age of landslides in the salt province is limited. Most landslides appear to have been active during oxygen isotope stages 2, 3, and 4 (18,170-71,000 yr BP) when salt movement due to sediment loading was most active. The age of the most recent landslide is less well established. For example, Reference 2.4S.6-7 stated that that no major SMFs have occurred in the northwestern Gulf of Mexico in the Holocene (i.e., the last 10,000 years). Reference 2.4S.6-7 (p. 309) stated:

> "Studies of submarine slides invariable prompt the question: Is the slope now completely stabilized? It is clear that most sliding on the Texas-Louisiana slope occurred during the late Pleistocene lowstands of sea level when sedimentation rates on the upper slope were high. No major Holocene slides have been documented. Low rates of deposition may be a primary reason for the present stability over much of the upper slope, and a further indication that sediments are relatively stable."

However, Reference 2.4S.6-3 suggests the occurrence of at least one landslide during the Holocene, with “one unpublished age date of a sample below a thin landslide deposit (<3 m thick) indicates that it is younger than 6,360 yr BP.” Therefore, no major SMFs have been documented for the salt province in over 6,300 years.

With respect to dimensions of the East Breaks slump scar, estimates of width, length, area, and volume have varied with different studies. For example, Reference 2.4S.6-40 stated that the slump “consists of a 20-km wide head scarp initiated along the 150-meter isobath, a 55 km long erosional chute, ending in a 95x30 km accretionary lobe. Total extent of the feature is 160 km from the shelf edge to a depth of 1,500 m” and “slumped deposits extend over a 3,200-km^2 area with a volume on the order of 50-60 km^3.” Reference 2.4S.6-7 stated that “the East Breaks Slide is a prominent mass-transport feature. Revised bathymetry shows that the slide originated on the upper slope (200-1000 m), in front of a sandy late Wisconsinan shelf-margin delta, where the gradient is up to 3°. It was deposited in a middle slope position (1000-1500 m) where the gradient is about 0.5°. Side-scan sonar data indicates that the slide is a strongly backscattering feature extending more than 110 km downslope from the shelf edge.” Reference 2.4S.6-3 (p. 32) stated that “the largest of these failures occurs in the northwestern Gulf of Mexico, is 114 km long, 53 km wide, covers about 2,250 km^2, and has been interpreted to consist of at least two debris flows.”

Source parameters for the East Breaks slump were estimated using three arc-second bathymetry data from the National Geophysical Data Center (NGDC) (Reference 2.4S.6-41). Source parameters, including slump width, length, and thickness, were estimated using a Geographic Information Systems (GIS) environment (Figure 2.4S.6-5). Slump width was estimated to be approximately 13.4 km. The length of the erosional chute was estimated to about 42 km. Based on a transect across the erosional chute, slump thickness was estimated to be about 100 m (i.e., see Path Profile A to A’ in Figure 2.4S.6-5). With respect to slope, Reference 2.4S.6-40 stated that “initial failure of the slump took place on very low angle slopes of less than two degrees while present slump deposits have an average seafloor slope of one-degree.” While a vertical drop of 850 m over a length of 42 km indicates a bed slope of

approximately 1.1 degrees, local bed slopes measured in GIS using a longitudinal transect along the erosional chute indicate a local maximum slope of about 1.95°. Therefore, a maximum local slope of 2° was used for a conservative estimate. Similarly, initial depth of the slide was estimated conservatively using the 200-m and 1000-m bathymetry contour elevations. Therefore, initial depth was estimated to be 600 m (i.e., (200 m + 1000 m)/2) (Figure 2.4S.6-5). Total length of the slide was taken from Reference 2.4S.6-3 as 114 km.

With respect to simulations, tsunami modeling was performed with MOST. Validation of the MOST code is well established (Reference 2.4S.6-9). MOST is based on the following three phases of long wave evolution (Reference 2.4S.6-8):

(i) A “Deformation Phase” that generates the initial conditions for a tsunami by simulating ocean floor and corresponding free surface changes due to a forcing mechanism;

(ii) A “Propagation Phase” that propagates the generated tsunami across the deep ocean using Nonlinear Shallow Water (NSW) wave equations; and

(iii) An “Inundation Phase” that simulates the shallow ocean behavior of a tsunami by extending the NSW calculations using a multi-grid runup algorithm to predict coastal flooding and inundation.

Specification of an initial deformation condition was based on scaling a dipole wave (i.e., a wave with a dipolar structure). A dipole wave is similar to the structure of an N-wave (i.e., a tsunami with a leading negative or depression wave followed by a positive elevation wave). An initial dipole wave is characteristic of tsunamis from submarine landslides, and possibly all tsunamis (Reference 2.4S.6-14).

After specifying an initial deformation condition, the propagation phase is based on a simplified form of the Navier-Stokes equations referred to as the nonlinear shallow water (NSW) equations (Reference 2.4S.6-8). The NSW equations are solved numerically with a finite difference algorithm and a series of nested grids (Reference 2.4S.6-42).

Since tsunami wavelength becomes shorter during shoaling, a series of nested grids are required for maintaining resolution of the wave with decreasing water depth. Therefore, three grids (i.e., A, B and C) were used for the MOST simulations (Figure 2.4S.6-6). The grids were derived from NGDC topography and bathymetry data (Reference 2.4S.6-41). Grid spacing between nodes was equal to 12 arc-seconds, 6 arc-seconds, and 6 arc-seconds, respectively.

MOST uses a moving boundary calculation for estimating tsunami runup onto dry land. Details of the moving boundary are discussed in Reference 2.4S.6-43. While friction factors are not used in the propagation phase of MOST, a friction factor must be specified for the inundation phase. Following sensitivity simulations, this value was set equal to 0.01 (i.e., n=0.1). Reference 2.4S.6-2 states that “several studies show that an unsteady flow during runup is not very sensitive to changes in the roughness coefficient”, and that “any moving boundary computation induces numerical friction

near the tip of the climbing wave (except in a Lagrangian formulation)." However, this value was selected based on a series of sensitivity tests, where the most conservative value that could be used without numerical instability over the full duration of the simulation was selected.

Initial wave heights (i.e., initial elevation of the depression wave due to a slump) were estimated using the slump center of mass motion model described in Reference 2.4S.6-10 and Reference 2.4S.6-11. Source parameters documented in the paragraphs above and in Figure 2.4S.6-5 were used for estimating initial wave height. Specific gravity of the slump mass was assumed to be equal to 2. The 100-m thickness (T) with respect to the 600-m initial depth (h) (T/h=0.17) and the thickness relative to the 42 km length (b) of the erosional chute (T/b=0.002) suggests initial wave height from the East Breaks slump would be relatively small. Using the NGDC bathymetry data (Figure 2.4S.6-5), initial wave height for the East Breaks slump was estimated to be 7.9 m. Considering variability in interpreting landslide dimensions, the estimate of 7.9 m is similar to the "tsunami wave on the order of 7.6 meters" predicted by Reference 2.4S.6-40.

As noted in the preceding paragraphs, estimates of slump dimensions can vary considerably with different interpretations. Therefore, estimates of initial conditions (i.e., wave height and shape) are not easily replicable between investigators. Consequently, after establishing a range of possible wave heights from scaling studies in Reference 2.4S.6-11 and Reference 2.4S.6-14, initial dipole conditions were developed for the East Breaks slump simulations by using SMF wave shapes developed for other SMF events. These events include the Palos Verdes (PV) landslide in Southern California (Reference 2.4S.6-12) and the 1998 Papua New Guinea (PNG) slump in the Sandaun Province (Reference 2.4S.6-13).

Scaled initial conditions were used for the simulations as relatively little data exists for SMFs, and the PV and PNG events have been tested extensively by the tsunami community (Reference 2.4S.6-13 and Reference 2.4S.6-14). Four scenarios were modeled as candidate PMT events. Candidate PMT events included waves with high initial wave heights relative to wavelength (i.e., steep waves), and waves with high initial wave heights relative to width. Minimum (negative) and maximum (positive) elevations of the initial wave deformations are listed in Table 2.4S.6-5. Steep wave scenarios included PV and PV(x20); wide wave scenarios included PNG and a hypothetical "Monster "condition." PV, which has a deformation area of 411 km^2, was developed as a minimum estimate of initial wave height for the East Breaks slump (Table 2.4S.6-5). PV(x20), which is PV scaled in elevation by twenty times and with a slightly smaller deformation area of 387 km^2, was developed as a maximum estimate of initial wave height for the East Breaks slump. PNG is scaled directly from the Papua New Guinea submarine slump described in Reference 2.4S.6-13, and has a deformation area of 879 km^2, which is about twice as large as PV. A hypothetical "Monster" condition was also developed as a complementary case for the East Breaks slump. The hypothetical "Monster" condition has not been tested by the tsunami community. Rather, the hypothetical "Monster" case was developed as a complementary case for the East Breaks slump to test a very wide initial wave (i.e.,

initial deformation area of 9932 km^2 or 3835 mi^2). All initial conditions were located at the centroid of the slump and oriented to relative to the slump direction.

MOST output includes maximum runup estimates (i.e., maximum inland elevation inundated by the tsunami above MSL). Maximum runup ranges from 1 to 2 m (3.28 to 6.56 ft, respectively) MSL for the South Texas Coast near STP 3 & 4 (Table 2.4S.6-5). The simulations indicate that a landslide tsunami originating from the East Breaks slump location would be unlikely to cross the barrier islands and produce a runup in excess of 2 m (6.56 ft) MSL. Plots of maximum wave amplitude relative to South Texas coast bathymetry are shown for PV, PV(x20), PNG, and the hypothetical "Monster" cases in Figure 2.4S.6-15, Figure 2.4S.6-17, Figure 2.4S.6-19, and Figure 2.4S.6-21, respectively. Time series of wave amplitude for a buoy located near the South Texas Coast for the PV, PV(x20), PNG, and hypothetical "Monster" are shown in Figure 2.4S.6-16, Figure 2.4S.6-18, Figure 2.4S.6-20, and Figure 2.4S.6-22, respectively.

Maximum drawdown was estimated at a buoy located at depth of 8.1 m and approximately 1 mi offshore of the South Texas coast (Figure 2.4S.6-4). At this location, significant drawdown of the water surface below MSL occurred for initial negative waves for the PV(x20) and hypothetical "Monster" scenarios. Maximum drawdown for the PV(x20) case had a duration of about 21 minutes, with a peak negative wave elevation of about -1.5 m (-4.9 ft) (Figure 2.4S.6-18). Maximum drawdown (i.e., below MSL) for the hypothetical "Monster" case had a duration of about 23 minutes, with a peak negative wave elevation of about -2.5 m (-8.2 ft) (Figure 2.4S.6-22). Therefore, maximum drawdown levels are not expected to impact any safety-related facilities at STP 3 & 4.

2.4S.6.5 Tsunami Water Levels

Reference 2.4S.6-3 (p. 34) stated that subaerial landslides, volcanogenic sources, and nearfield intraplate earthquakes are unlikely to be the causative tsunami generator for damaging tsunamis in the Gulf of Mexico region. Reference 2.4S.6-3 also stated that far-field "tsunamis generated by earthquakes do not appear to impact the Gulf of Mexico coast." Simulations by Reference 2.4S.6-4 of postulated "worst-case" seismic events reported a tsunami near STP 3 & 4 with a shoreline amplitude of 0.15 m.

As far-field tsunamis are unlikely to impact the South Texas coast, the PMT for STP Subsection 2.4S.6 is defined as a tsunami occurring from a near-field submarine landslide near the East Breaks slump. Using the MOST code (Reference 2.4S.6-8), a series of scaled initial conditions were used to assess the near-field hazard of tsunami generation from submarine landslides to the STP 3 & 4 site. For scenarios with wave heights ranging from - 140 m (-459 ft) to 60 m (197 ft) and deformation areas ranging from 410 km^2 to 9932 km^2, tsunami waves from the SMFs were diffused rapidly by the continental shelf offshore of the South Texas coast. The remaining wave energy that reached the South Texas coast was largely reflected by the barrier islands. For example, maximum predicted runup from the simulations did not exceed 2 m. Maximum flow depth from the simulations, which occurred at the shoreline, did not exceed 3.25 m. Maximum rundown did not exceed 2.5 m about 1 mi offshore of the South Texas coast.

The initial deformation conditions listed in Table 2.4S.6-5 plausibly exceed wave heights from propagating tsunamis that may occur due to landslides in remote areas of the Gulf of Mexico. For example, relative to the location of STP 3 & 4, most SMF sources in the Gulf of Mexico are mid-field to far-field sources (i.e., source locations over 200 km away) (Figure 2.4S.6-3). The distance from STP 3 & 4 to the East Breaks slump is 142 km (88.2 mi). The distance from STP 3 & 4 to Bryant Canyon is 517 km (321.2 mi). The distance from STP 3 & 4 to Mississippi Canyon and the Eastern Mississippi Canyon/Fan is 640 km (397.7 mi) and 709 km (440.6 mi), respectively. The distance from STP 3 & 4 to the Campeche Escarpment and Bay of Campeche is 873 km (542.5 mi) and 953 km (592.2 mi), respectively. The distance from STP 3 & 4 to the Florida escarpment is 1169 km (726.4 mi). Since landslide waves tend to be steep (i.e., high initial wave height relative to wavelength) and are prone to breaking, wave heights at the East Breaks slump from mid-field and far-field sources are not expected to exceed the simulated initial conditions. As shown with the simulations, diffusion and energy dissipation from large SMF events is likely to be significant. Therefore, potential runup from these events is likely to be lower than the scenarios modeled for the East Breaks slump, and additional landslide scenarios in the Gulf of Mexico are not further considered.

As discussed earlier, the maximum flood level for a PMT event also included an analysis of the 10% exceedance of the astronomical high tide and long-term sea level rise. As regulatory criteria for these components are only available for the Probable Maximum Storm Surge (PMSS), the criteria for the PMSS in Regulatory Guide 1.59 (1977) (Reference 2.4S.6-15) were adopted for the PMT analysis. Based on tide gage data for NOS Station #8772440, the 10% exceedance of the astronomical high tide was estimated to be 3.54 ft MSL (Reference 2.4S.6-16). The long-term sea level rise for this station was estimated by NOAA to be 1.43 ft per century (Reference 2.4S.6-17). The peak flood level due to a probable maximum tsunami event is therefore estimated to be of the order of 11.5 ft MSL within the next century.

With respect to the assumption of the MSL datum (or NGVD 29) shift relative to actual mean sea level from tidal measurements, it should be noted that the Freeport, Texas, tide gage does not have a published or official NGVD29 orthometric height mark. Since the one mark that does exist suggests the difference between MSL (or NGVD 29) to actual mean sea level is small (i.e., within ±0.2 ft of the Mean Lower-Low Water datum), the shift to MSL (or NGVD 29) should be considered as a reasonable approximation of the actual value.

Based on the discussion above, it is concluded that the probable maximum tsunami event will not be the controlling design basis flood event for STP 3 & 4 because the postulated flood level is lower than the design basis flood elevation of 40.0 feet MSL predicted for a hypothetical breach event of the MCR embankment as described in Section 2.4S.4. Coincident wind waves are not considered in the analysis since it is evident that the PMT event will have no flooding impacts on safety-related facilities of STP 3 & 4.

2.4S.6.6 Hydrography and Harbor or Breakwater Influences on Tsunami

Because the STP 3 & 4 site is over fifteen miles inland from the South Texas coast and barrier islands, and the postulated maximum flood level of no more than 11.5 ft MSL due to the PMT event is lower than the site grade elevations of 32 ft MSL to 36.6 ft MSL for the power block area of STP 3 & 4, there will be no local onsite effects associated with different tsunami types, including breaking waves, bores, or any resonance effects that would result in higher tsunami runup on the safety-related facilities. Therefore, no additional analysis of the translation of tsunami waves from offshore generator locations to the site is warranted.

2.4S.6.7 Effects on Safety-Related Facilities

The postulated maximum flood level of no more than 11.5 ft MSL due to the PMT event is lower than the site grade elevations of 32 ft MSL to 36.6 ft MSL for the power block area of STP 3 & 4. Therefore, the PMT event will have no flooding impacts on safety-related facilities or the design basis functions of STP 3 & 4, and there will be no impact of debris and water-borne projectiles and impacts of sediment erosion and deposition on the safety-related facilities of STP 3 & 4.

2.4S.6.8 References

2.4S.6-1 “Tsunami Hazard Assessment at Nuclear Power Plant Sites in the United States of America,” Prasad, R. and Pacific Northwest National Laboratory (PNNL), NUREG CR-6966, PNNL-17397, Nuclear Regulatory Commission, Draft Report for Comment, Revision: August 2008.

2.4S.6-2 “Scientific and Technical Issues in Tsunami Hazard Assessment of Nuclear Power Plant Sites,” González et al., F.I., Bernard, E., Dunbar, P., Geist, E., Jaffe, B., Kanoglu, U., Locat, J., Mofjeld, H., Moore, A., Synolakis, C.E., Titov, V. and R. Weiss (Science Review Working Group), National Oceanic and Atmospheric Administration (NOAA) Technical Memorandum OAR Pacific Marine Environmental Laboratory 136, 2007.

2.4S.6-3 “Evaluation of Tsunami Sources with the Potential to Impact the U.S. Atlantic and Gulf Coasts - A Report to the Nuclear Regulatory Commission: U.S. Geological Survey Administrative Report,” Atlantic and Gulf of Mexico Tsunami Hazard Assessment Group, Revision: August 22, 2008.

2.4S.6-4 “Model Predictions of Gulf and Southern Atlantic Coast Tsunami Impacts from a Distribution of Sources,” Knight, B. 2006, Science of Tsunami Hazards 24(2): 304-312.

2.4S.6-5 “Cumbre Vieja Volcano - Potential Collapse and Tsunami at La Palma, Canary Islands,” Ward, S. N. and S. Day. 2001. Geophysical Research Letters 28(17): 3397-3400.

2.4S.6-6 “Geomorphology and age of the Oxygen isotope stage 2 (last lowstand) sequence boundary on the northwestern Gulf of Mexico continental shelf," Simms, A.R., Anderson, J.B., Milliken, K.T., Taha, Z.P., Wellner, in Seismic Geomorphology: Applications to Hydrocarbon Exploration and Production, Davies, R.J. , Posamentier, H.W., Wood, L. J. & Cartwright, J. A. (eds.), Geological Society, London, Special Publications, 277: 29-46, 2007.

2.4S.6-7 "Sedimentary Features of the South Texas Continental Slope as Revealed by Side-Scan Sonar and High-Resolution Seismic Data,” Rothwell, R.G., Kenyon, N.H. and B.A. McGregor, The American Association of Petroleum Geologists Bulletin 75(2): 298-312, 1991.

2.4S.6-8 “Implementation and testing of the Method of Splitting Tsunami (MOST) model,” Titov, V.V., and F.I. González et al., NOAA Technical Memorandum ERL PMEL112, Pacific Marine Environmental Laboratory, 1997.

2.4S.6-9 “Tsunami Science Before and Beyond Boxing Day 2004,” Synolakis, C.E. and E.N. Bernard, Philosophical Transactions of the Royal Society 64: 2231-2265, 2006.

2.4S.6-10 “Tsunami Features of Solid Block Underwater Landslides,” Watts, P., Journal of Waterway, Port, Coastal, and Ocean Engineering 126(3): 144-152, 2000.

2.4S.6-11 “Tsunami Generation by Submarine Mass Failure, Part II, Predictive Equations and Case Studies,” Watts, P., Grilli, S.T., Tappin, D.R. and G.J. Fryer, Journal of Waterway, Port, Coastal, and Ocean Engineering 131(6): 298-310, 2005.

2.4S.6-12 “Tsunami Hazards in Southern California,” Borrero, J.C., Ph.D. Thesis, University of Southern California, 2002.

2.4S.6-13 “The Slump Origin of the 1998 Papua New Guinea Tsunami,” Synolakis, C.E., Bardet, J.-P., Borrero, J.C., Davies, H.L., Okal, E.A., Silver, E.A., Sweet, S., and D.R. Tappin, Proceedings: Mathematical, Physical and Engineering Sciences 458(2020): 763-789, 2002.

2.4S.6-14 “Tsunami and Seiche,” Synolakis, C. E. 2004 from Earthquake Engineering Handbook, edited by Chen, W. F. and C. Scawthorn, CRC Press. 9-1 to 9-90.

2.4S.6-15 “Design Basis Floods for Nuclear Power Plants,” U.S. Nuclear Regulatory Commission, Regulatory Guide 1.59, Revision 2, 1977.

2.4S.6-16 “NOS Station #8772440, Freeport - Verified Historic Tide Data,” National Oceanic and Atmospheric Administration (NOAA), available at http://tidesandcurrents.noaa.gov/data_menu.shtml?stn=8772440%20Freeport,%20 TX&type=Historic+Tide+Data, accessed August 19, 2008.

2.4S.6-17 "NOS Station #8772440, Freeport - Sea Level Trends," National Oceanic and Atmospheric Administration (NOAA), 2008, available at http://tidesandcurrents.noaa.gov/sltrends/sltrends_station.shtml?stnid=8772440%2 0Freeport,%20TX, accessed August 19, 2008.

2.4S.6-18 "Tsunami Data at NGDC," National Geophysical Data Center/World Data Center. Available at http://www.ngdc.noaa.gov/hazard/tsu.shtml, accessed November 22, 2008.

2.4S.6-19 "Caribbean Tsunamis: A 500-Year History from 1498-1999. Kluwer Academic Publishers," O' Loughlin, K. F. and J. F. Lander. 2003. The Netherlands. 280 pp.

2.4S.6-20 "Tsunamis and Tsunami-Like Waves of the Eastern United States," Science of Tsunami Hazards 20(3): 120-157, Lockridge, P. A., Lowell, S. W., and J. F. Lander. 2002.

2.4S.6-21 "Improving Earthquake and Tsunami Warnings for the Caribbean Sea, the Gulf of Mexico, and the Atlantic Coast," USGS Fact Sheet 2006-3012, United States Geological Survey, 2006.

2.4S.6-22 "NOAA Center for Tsunami Research," Pacific Marine Environmental Laboratory (PMEL). Available at http://nctr.pmel.noaa.gov/, accessed November 23, 2008.

2.4S.6-23 "A Brief History of Tsunamis in the Caribbean Sea. Science of Tsunami Hazards," 20(2): 57-94, Lander, J. F., Whiteside, L. S., and P. A. Lockridge, 2002.

2.4S.6-24 "Unusual Tide Registration of Earthquake,"Parker, W.E. 1922. Bulletin of the Seismological Society in America, pp. 28-30.

2.4S.6-25 "Earthquake History of Puerto Rico, Seismicity Investigation," Appendix I, Part A, An Earthquake History of Puerto Rico, Aguirre Nuclear Power Plant, Weston Geophysical Research," Campbell, J.B., 1972, Weston, Massachusetts.

2.4S.6-26 "Alaska Earthquake of 27 March 1964: Remote Seiche Stimulation. Science 145: 261-262," Donn, W. L. 1964.

2.4S.6-27 "Historical Earthquakes, Prince William Sound, Alaska," United States Geological Survey, Available at http://earthquake.usgs.gov/regional/states/events/ 1964_03_28.php, accessed April 27, 2007.

2.4S.6-28 "Seismic Seiches in Bays, Channels, and Estuaries, from The Great Alaska Earthquake of 1964: Oceanography and Coastal Engineering," McGarr, A. and R. C. Vorhis. 1972, National Academy of Sciences, Washington, D.C. 25-28.

2.4S.6-29 "Assessment of Source Probabilities for Potential Tsunamis Affecting the U.S. Atlantic Coast," Parsons, T., Geist, E.L., in press, Marine Geology, doi:10.1016/j.margeo.2008.08.005.

2.4S.6-30 "Global Centroid Moment Tensor (CMT)," Available at http://www.globalcmt.org/, accessed November 21, 2008.

2.4S.6-31 "Numerical Modeling of the Global Tsunami: Indonesian Tsunami of 26 December 2004", Kowalik, Z., Knight, W., Logan, T. and P. Whitmore, Science of Tsunami Hazards 23(1): 40-56, 2005.

2.4S.6-32 "Surface Deformation Due to Shear and Tensile Faults in a Half-Space," Okada, Y., Bulletin of the Seismological Society of America 75(4): 1135-1154, 1985.

2.4S.6-33 "Magnitude 5.8 Gulf of Mexico Earthquake of 10 September 2006," National Earthquake Information Center, United States Geological Survey, Available at http://earthquake.usgs.gov/eqcenter/eqinthenews/2006/usslav/#summary, accessed December 02, 2008.

2.4S.6-34 "Magnitudes and locations of the 1811-1812 New Madrid, Missouri, and the 1886 Charleston, South Carolina, Earthquakes," Bakun, W. H. and M. G. Hopper. 2004. Bulletin of the Seismological Society of America 94(1): 64-75.

2.4S.6-35 "Modeling the La Palma Landslide Tsunami," Mader, C.L., Science of Tsunami Hazards 19(3): 150-170, 2001.

2.4S.6-36 "SAGE calculations of the tsunami threat from La Palma," Gisler, G., Weaver, R. and M.L. Gittings, 2006, Science of Tsunami Hazards 24(4): 288-301.

2.4S.6-37 "The Threat Posed by the Tsunami to the UK," British Geology Society, 2005. Study commissioned by Debra Flood Management, 133 pp.

2.4S.6-38 "Addressing the Challenges in the Placement of Seafloor Infrastructure on the East Breaks Slide-A Case Study: The Falcon Field (EB 579/623)," Hoffman, J.S., Kaluza, M.J., Griffiths, R., Hall, J. and T. Nguyen, Northwestern Gulf of Mexico, Offshore Technology Conference 16748, 2004.

2.4S.6-39 "Downslope Sediment Transport Processes and Sediment Distributions at the East Breaks, northwest Gulf of Mexico," Piper, J.N., and Behrens, in Proceedings of the 23rd Annual Gulf Coast Section SEPM Research Conference, Houston, Texas, pp. 359-385, 2003.

2.4S.6-40 "East Breaks Slump, Northwest Gulf of Mexico," Offshore Technology Conference, OTC paper 12960, Trabant, P., Watts, P., Lettieri, F. and G. Jamieson. 2001.

2.4S.6-41 National Geophysical Data Center (NGDC), 2008, “Bathymetry, Topography, and Relief,” National Oceanic and Atmospheric Administration (NOAA), available at http://www.ngdc.noaa.gov/mgg/bathymetry/relief.html, accessed October 5, 2008.

2.4S.6-42 Titov, V.V. and C.E. Synolakis, 1998, “Numerical Modeling of Tidal Wave Runup,” Journal of Waterway, Port, Coastal, and Ocean Engineering 124(4): 157- 171.

2.4S.6-43 Titov, V.V., 1997, Numerical Modeling of Long Wave Runup, Ph.D. Thesis, University of Southern California, Los Angeles, California, 141 pp.

Table 2.4S.6-1 Approximate range of tsunami parameters in the deep ocean (Reference 2.4S.6-2).

Parameter	Minimum	Maximum
Depth	1000 m	5000 m
Period	5 min	60 min
Amplitude	0.01 m	1 m
Wavelength	30 km	800 km
Speed	0.10 km/s	0.22 km/s
Max Current	0.05 cm/s	9.9 cm/s

Table 2.4S.6-2 Approximate range of tsunami parameters in shallow water (Reference 2.4S.6-2).

Parameter	Minimum	Maximum
Depth	10 m	1000 m
Period	5 min	60 min
Amplitude	1 m	10 m
Wavelength	3 km	356 km
Speed	0.01 km/s	0.10 km/s
Max Current	9.9 cm/s	990 cm/s

Table 2.4S.6-3 Areas of potential seismic tsunamigenesis in the Caribbean (Reference 2.4S.6-3, pp. 105 and 107).

Caribbean Source	Latitude (° N)	Longitude (° W)
North Panama Deformation Belt	9-12	83-77
Northern South American Convergent Zone	11.5-14	77-64

Table 2.4S.6-4 Source parameters for Veracruz scenario.

Epicenter	M_w	Rupture Length (km)	Width (km)	Depth (km)	Strike (°)	Dip (°)	Rake (°)	Max slip (m)
20° N, 265° E	8.2	200	70	5	135	20	90	2

Table 2.4S.6-5 Initial wave deformation characteristics and maximum runup for simulations.

Case	Deformation Area (sq. km)	Dipole Initial Minimum (m below MSL)	Dipole Initial Maximum (m below MSL)	Maximum Runup (m above MSL)	Figure Reference
PV	411	-7	3	1	2.4S.6-7; 2.4S.6-8
PV(x20)	387	-140	60	2	2.4S.6-9; 2.4S.6-10
PNG	879	-20	16	2	2.4S.6-11; 2.4S.6-12
Monster	9932	-38	27	2	2.4S.6-13; 2.4S.6-14

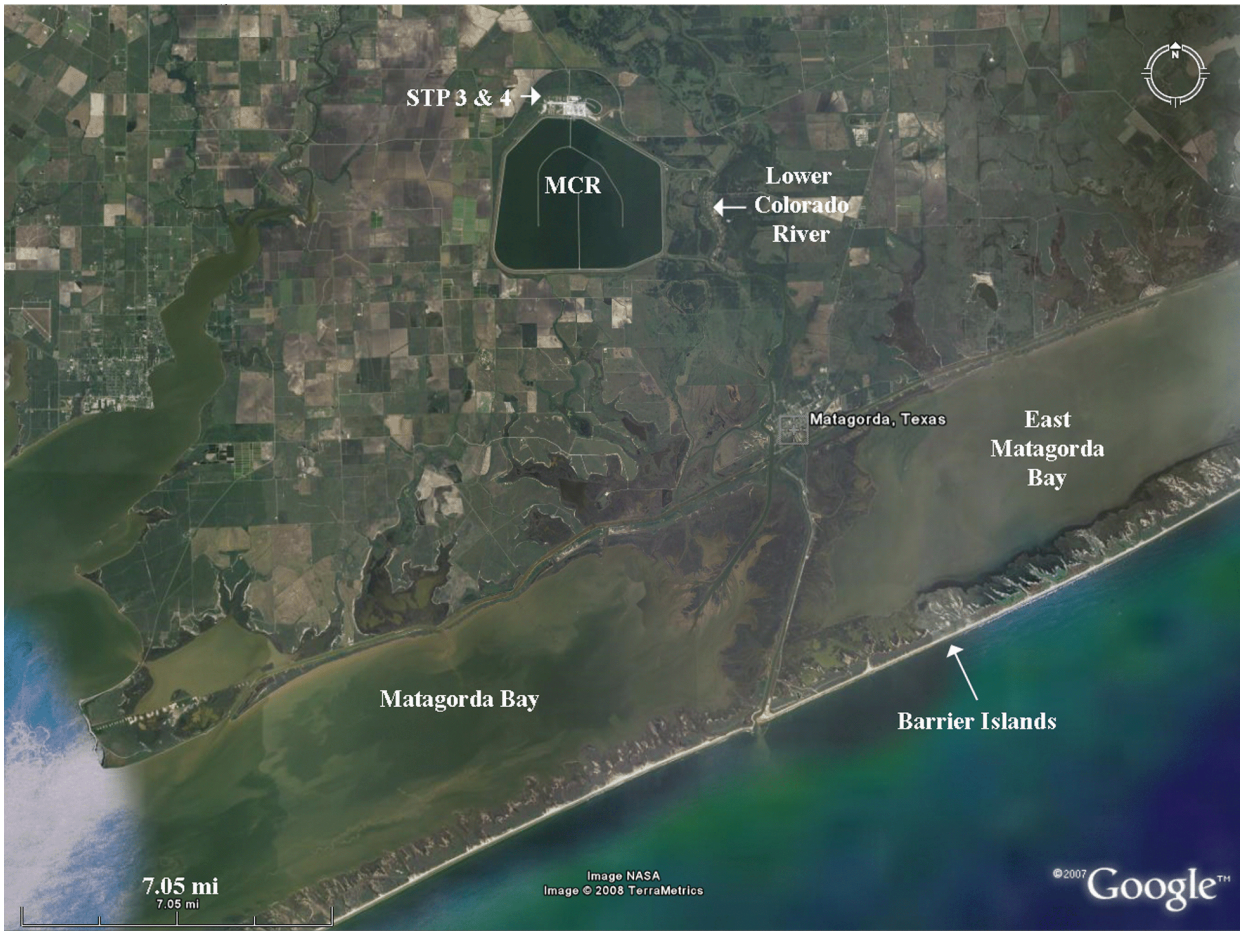

Figure 2.4S.6-1 Location Map of STP 3 & 4 from the Gulf Coast and Colorado River.

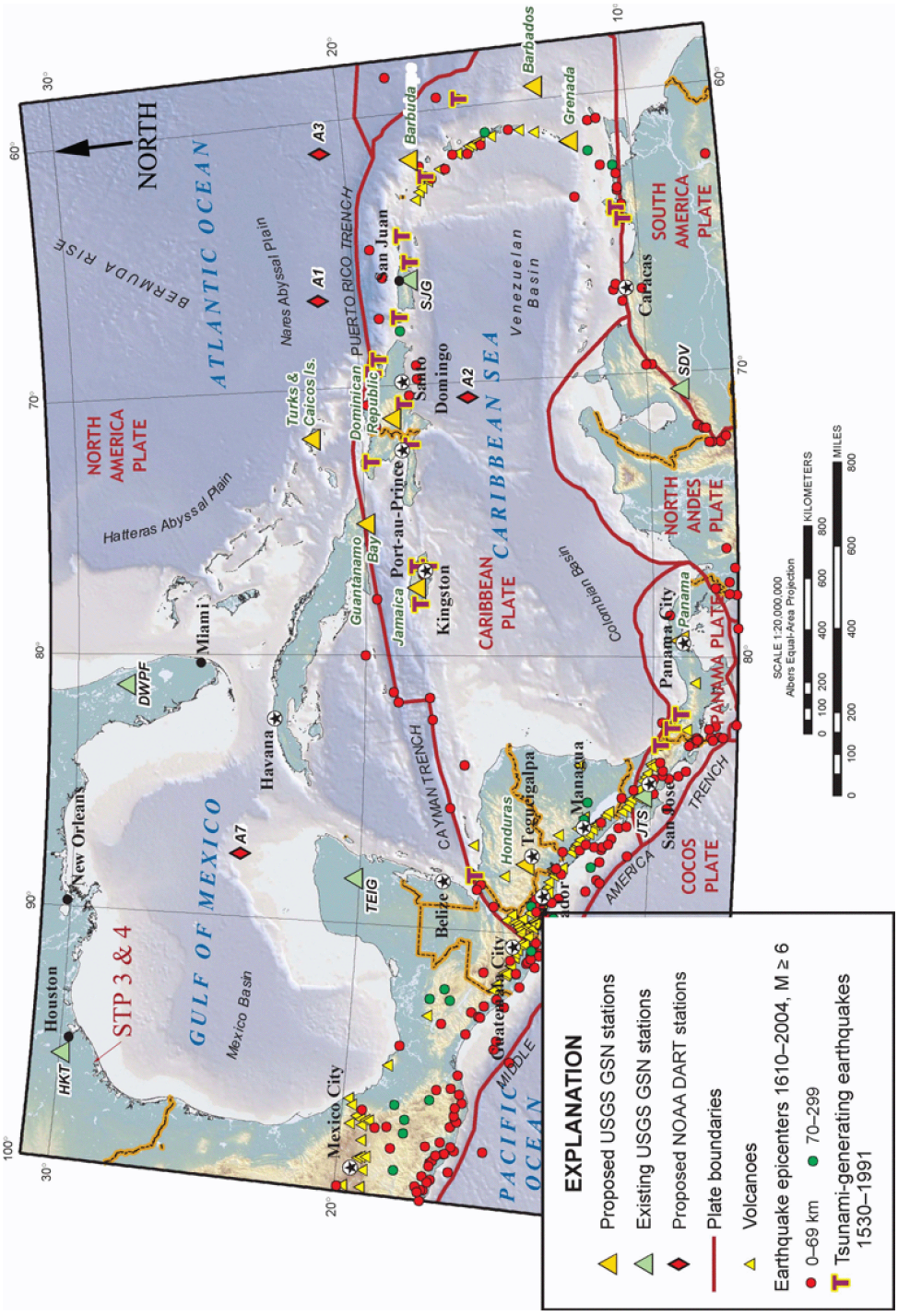

Figure 2.4S.6-2 Regional Map of Plate Boundaries and Tsunami-Generating Earthquakes from 1530-1991 in the Caribbean Sea (modified from Reference 2.4S.6-21).

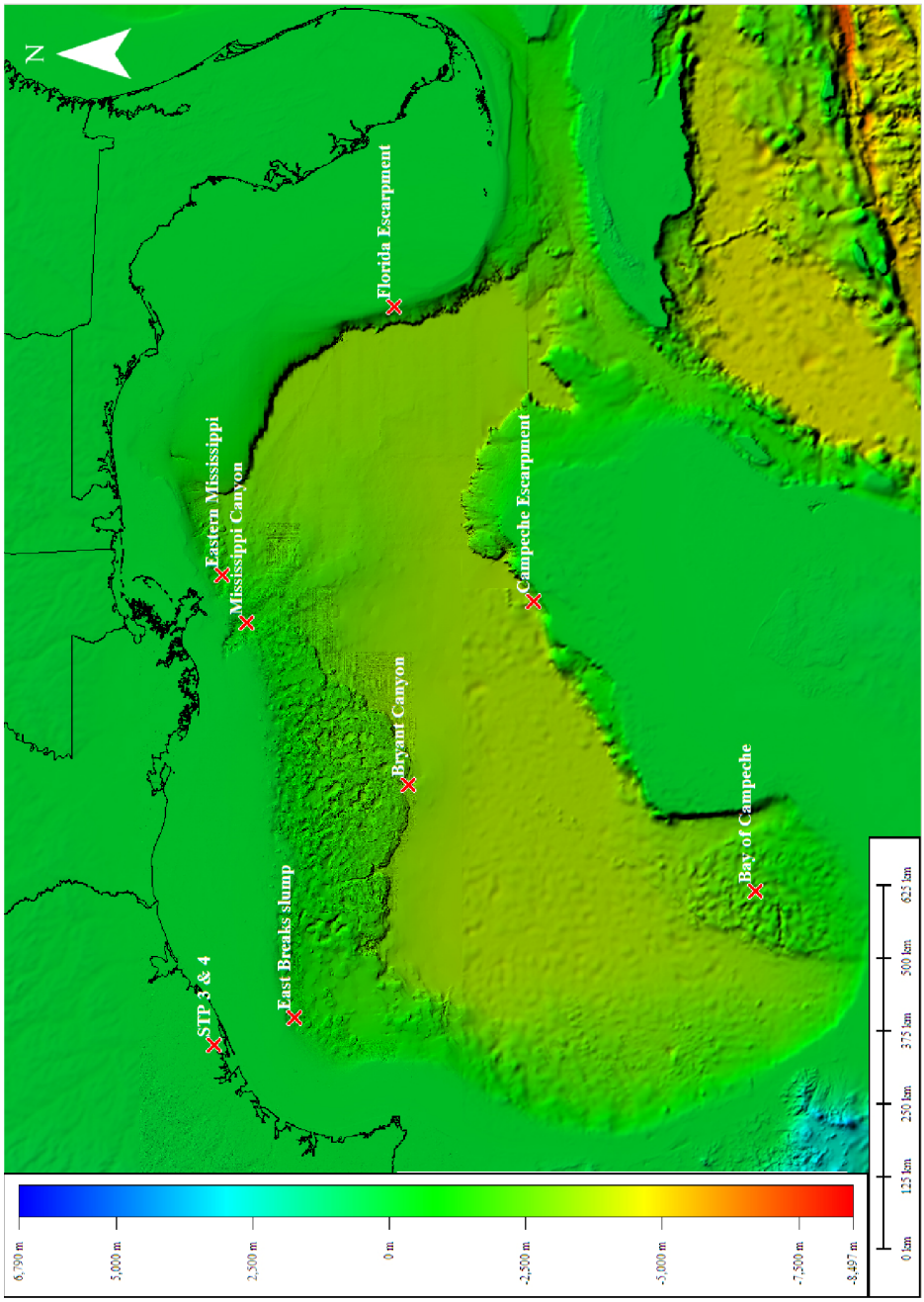

Figure 2.4S.6-3 Landslide source regions in Gulf of Mexico. At 142 km from STP 3 & 4, the East Breaks slump is the only near-field landslide source. Source of bathymetry: Reference 2.4S.6-41.

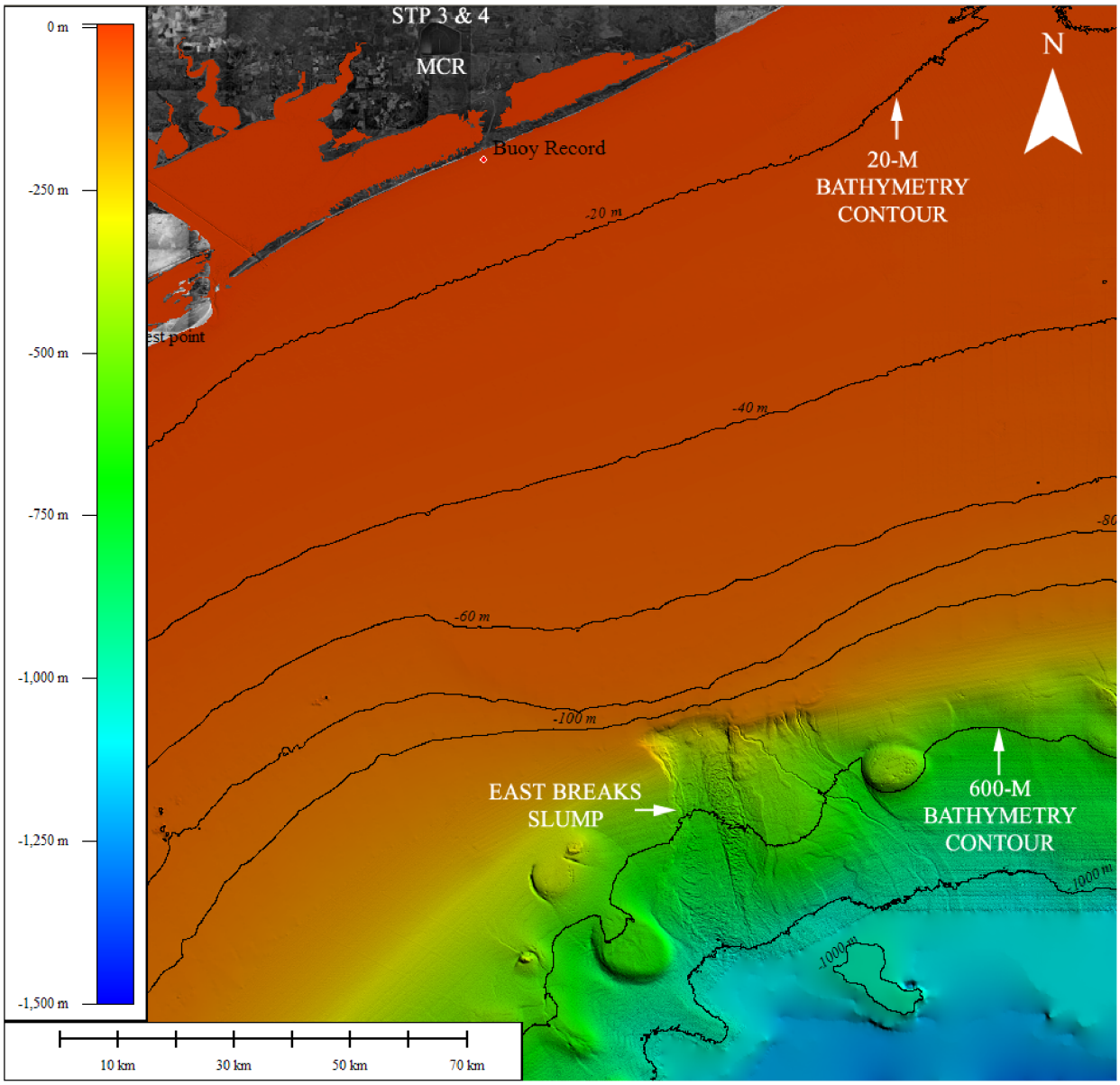

Figure 2.4S.6-4 Location of East Breaks slump relative to STP 3 & 4 (Source: Reference 2.4S.6-41). Buoy record for recording tsunami wave amplitudes is located at 28.58° N and 95.98° W. Bathymetry elevations are relative to Mean Sea Level (MSL).

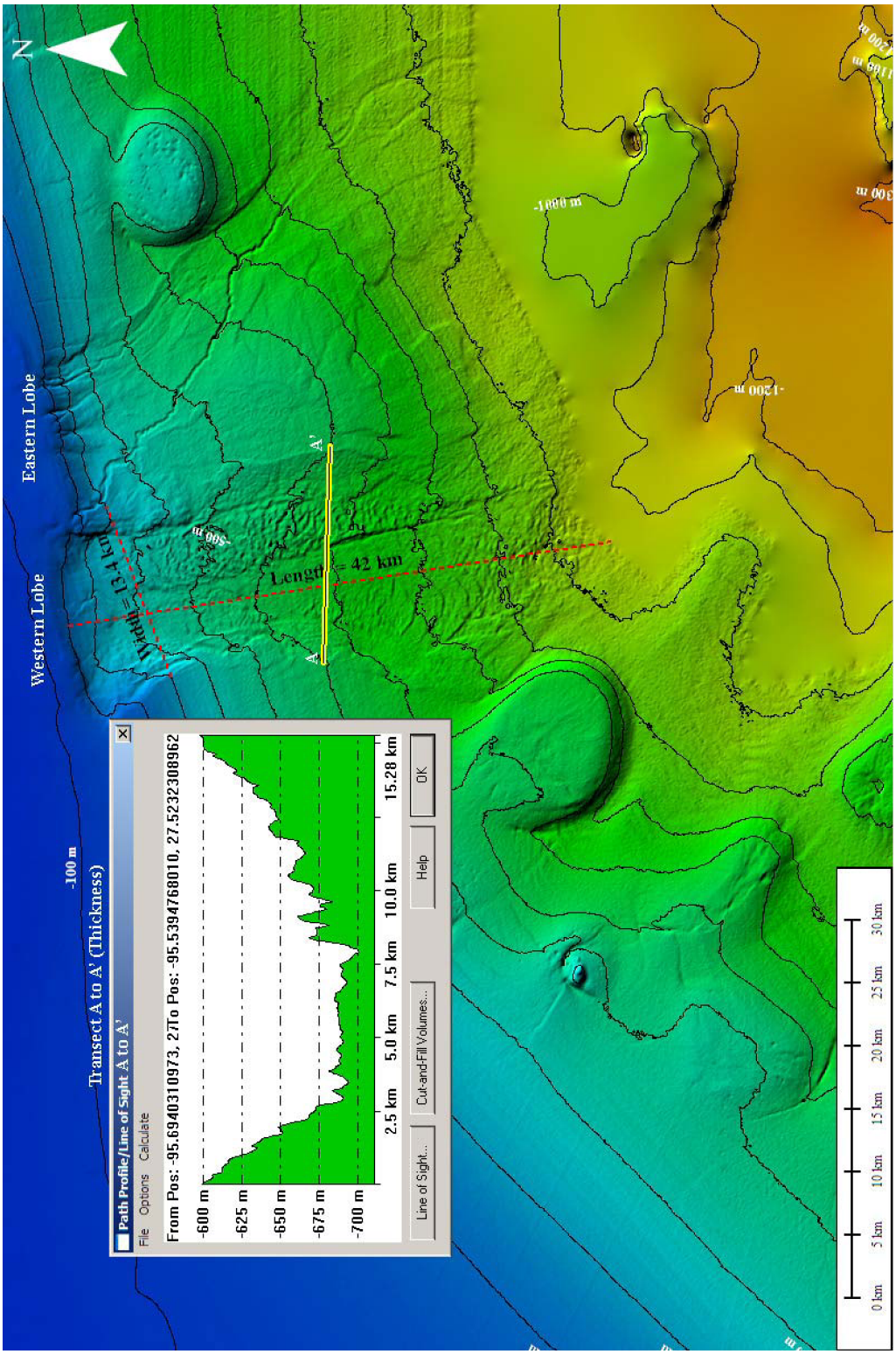

Figure 2.4S.6-5 Source parameters for East Breaks slump - Bathymetry elevations are relative to MSL. (Source of bathymetry data: Reference 2.4S.6-41)

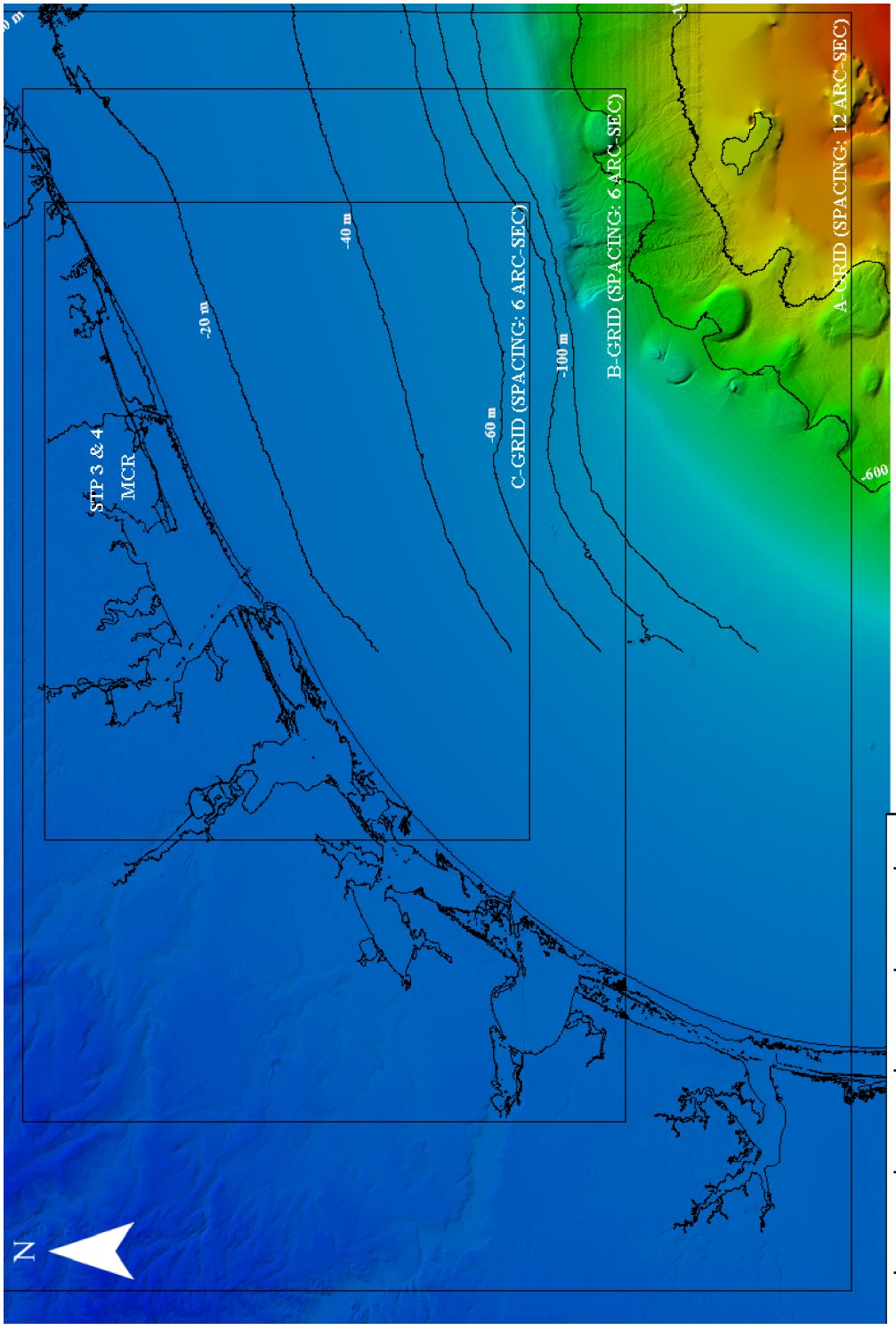

Figure 2.4S.6-6 Grid spacing for East Breaks slump modeling with MOST. Bathymetry elevations are relative to MSL. (Source of bathymetry data: Reference 2.4S.6-41)

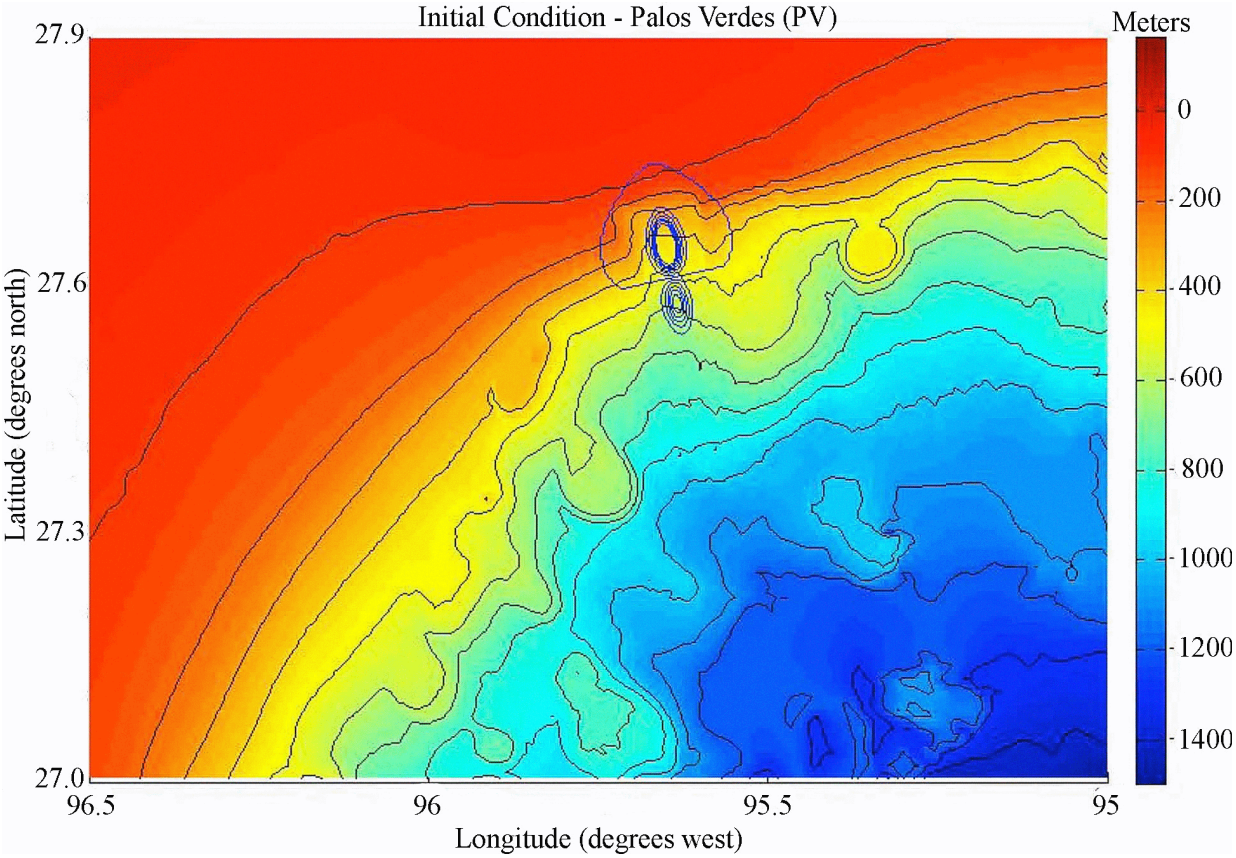

Figure 2.4S.6-7 Plan view of Palos Verdes (PV) initial deformation condition at location of the East Breaks slump in the Gulf of Mexico. Elevations of initial wave correspond with elevations in Figure 2.4S.6-8.

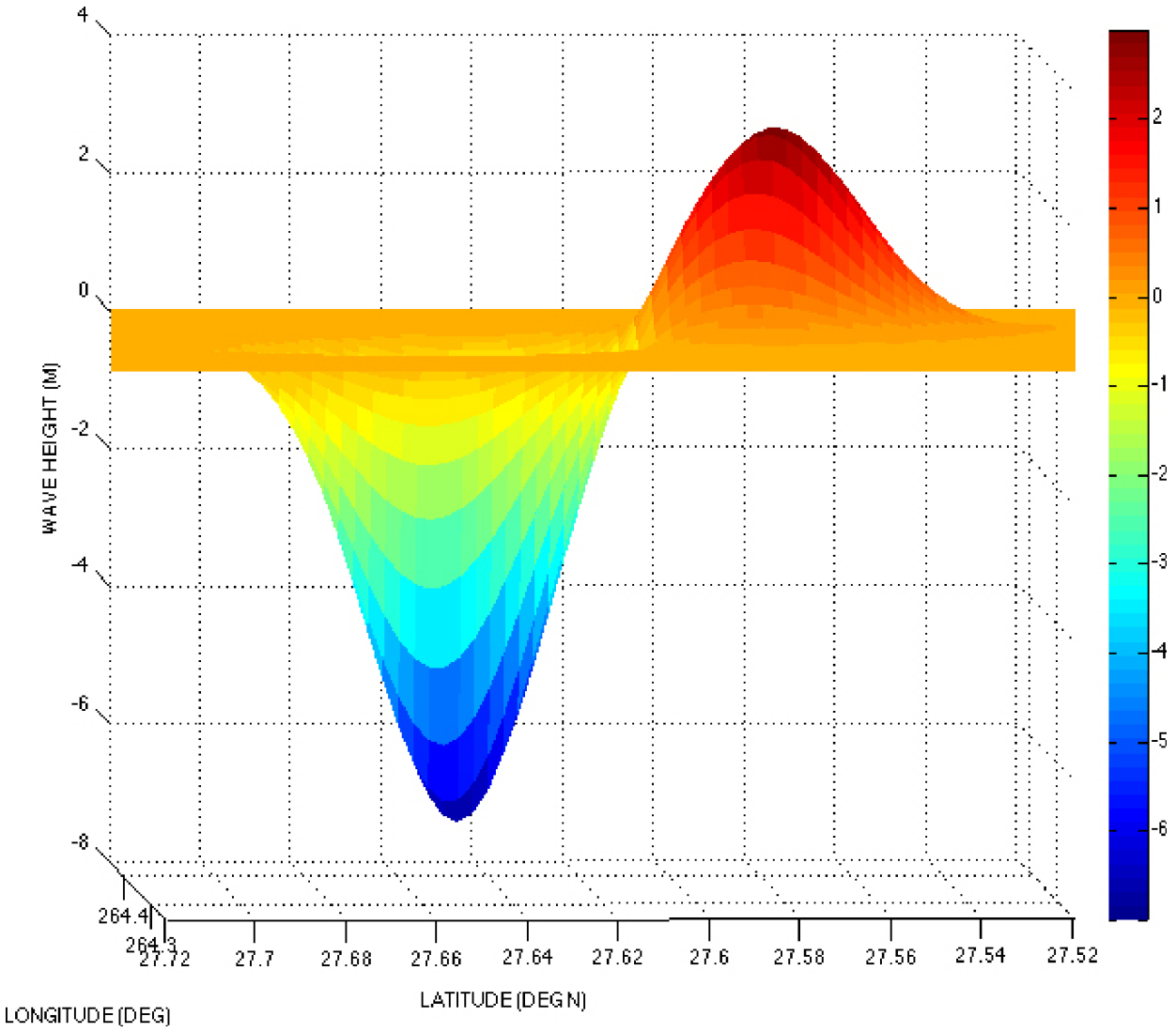

Figure 2.4S.6-8 Side view of Palos Verdes (PV) initial deformation condition. Maximum elevation of negative wave is -7 m (MSL); maximum elevation of positive wave is +3 m. (MSL).

Source: Reference 2.4S.6-5, p. 5

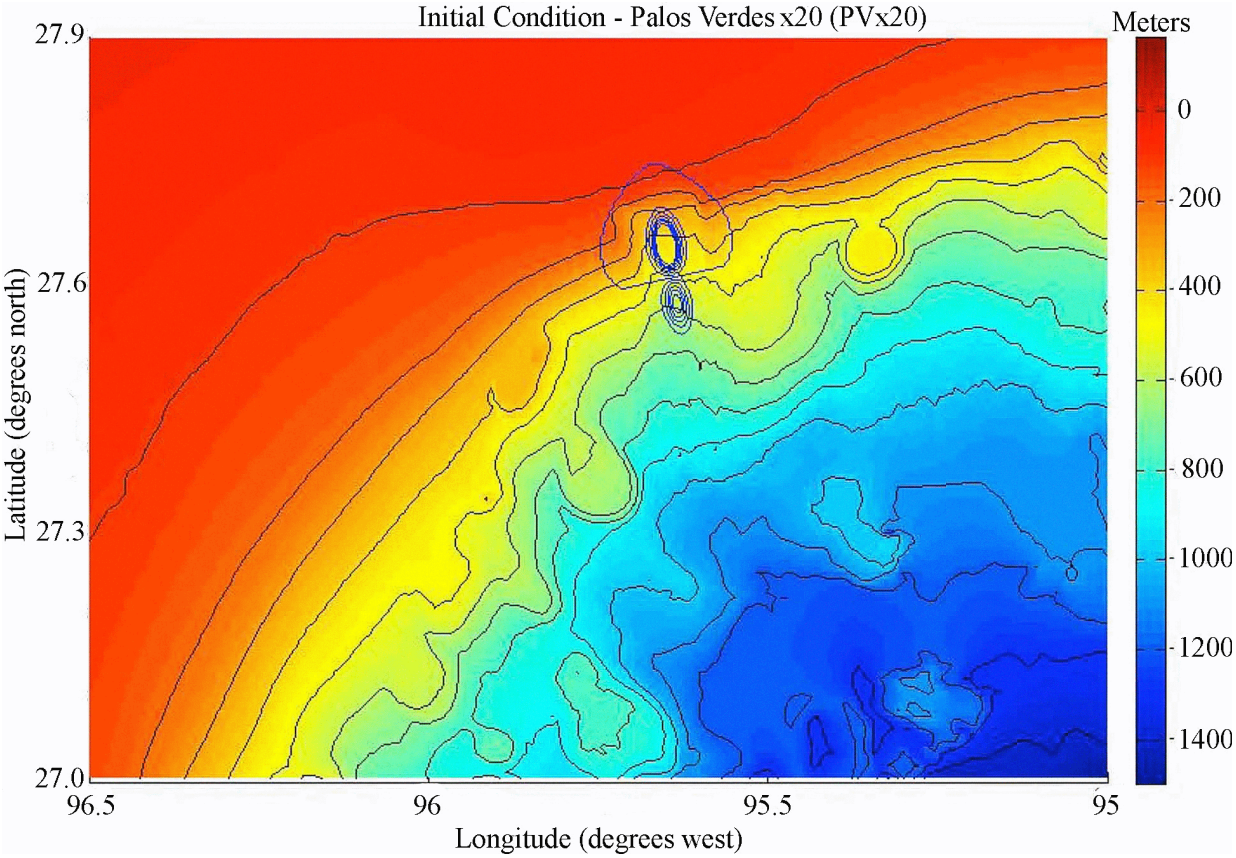

Figure 2.4S.6-9 Plan view of Palos Verdes x20 (PVx20) initial deformation condition at location of the East Breaks slump in the Gulf of Mexico. Elevations of initial wave correspond with elevations in Figure 2.4S.6-10.

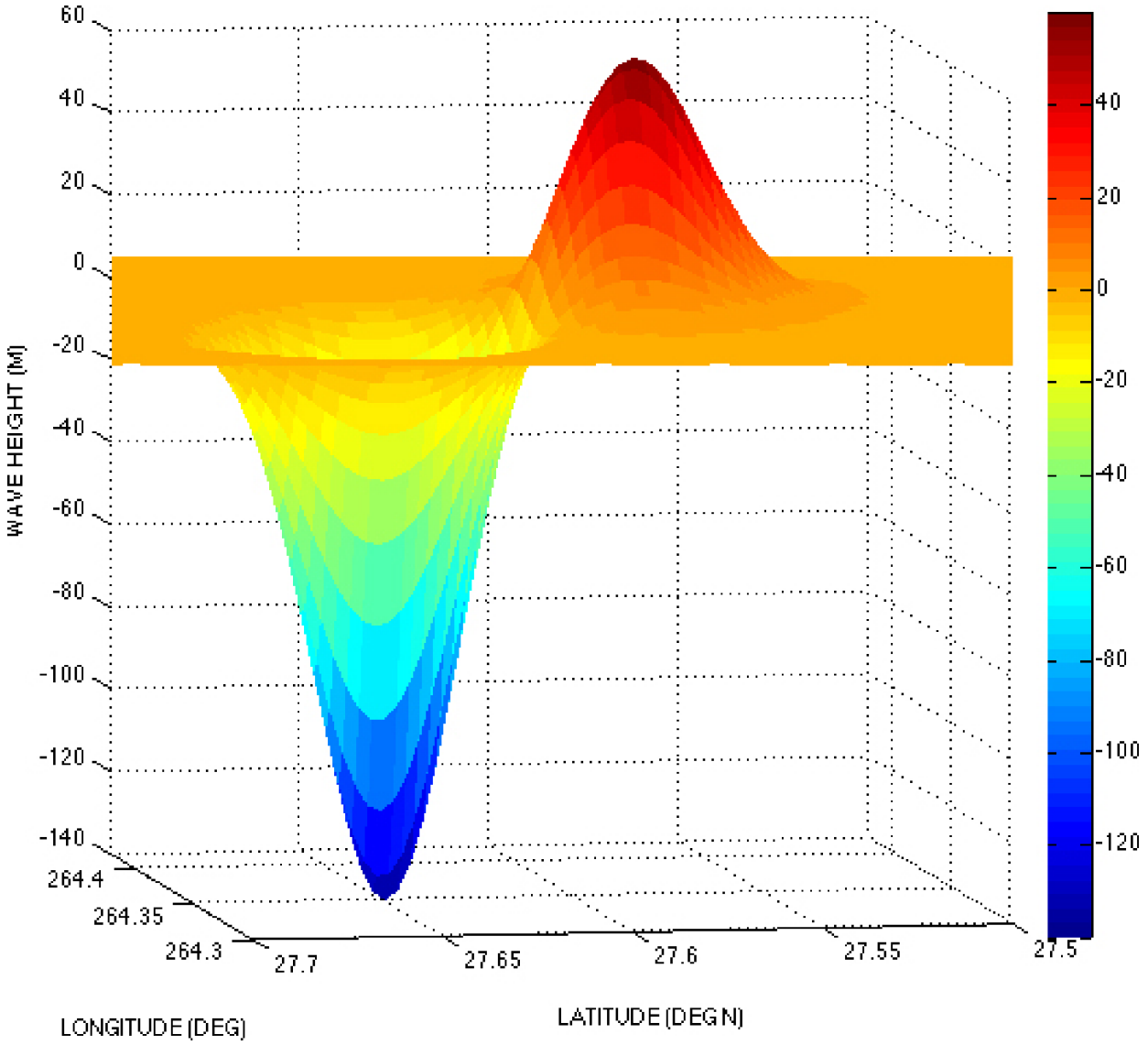

Figure 2.4S.6-10 Side view of Palos Verdes x20 (PVx20) initial deformation condition. Maximum elevation of negative wave is -140 m (MSL); maximum elevation of positive wave is +60 m (MSL).

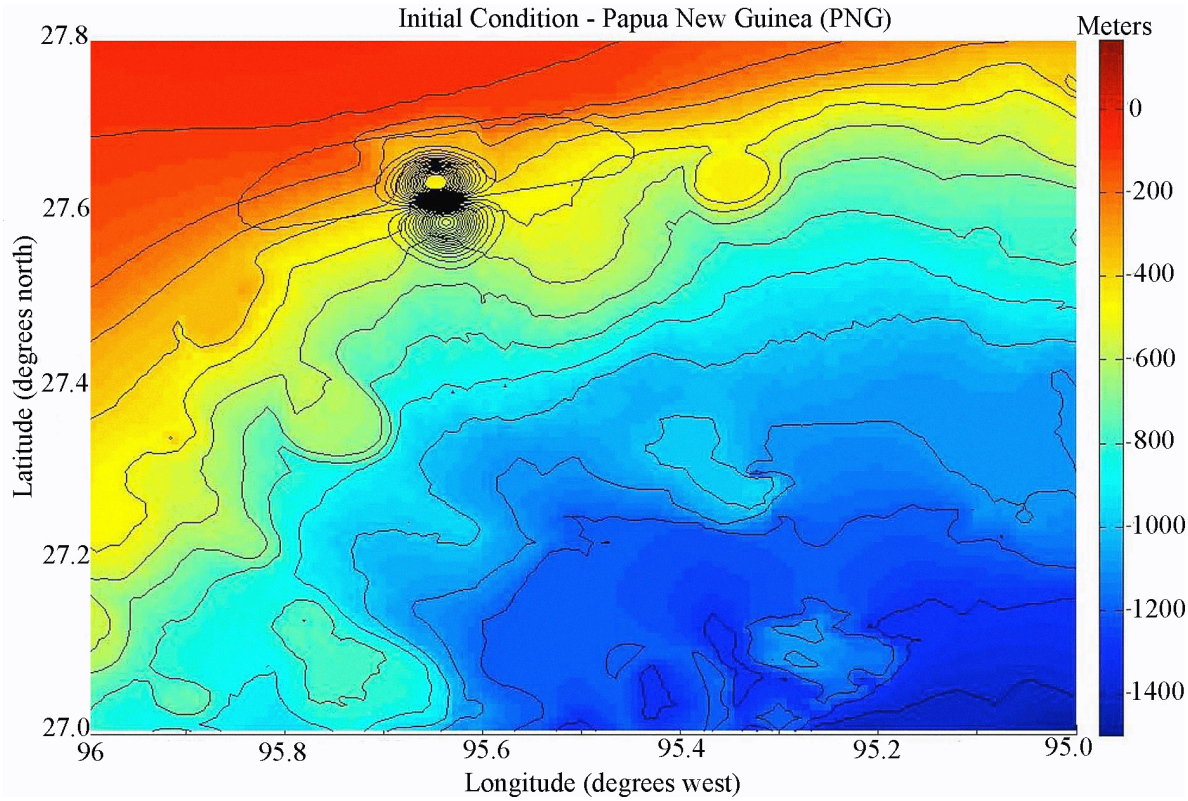

Figure 2.4S.6-11 Plan view of Papua New Guinea (PNG) initial deformation condition at location of the East Breaks slump in the Gulf of Mexico. Elevations of initial wave correspond with elevations in Figure 2.4S.6-12.

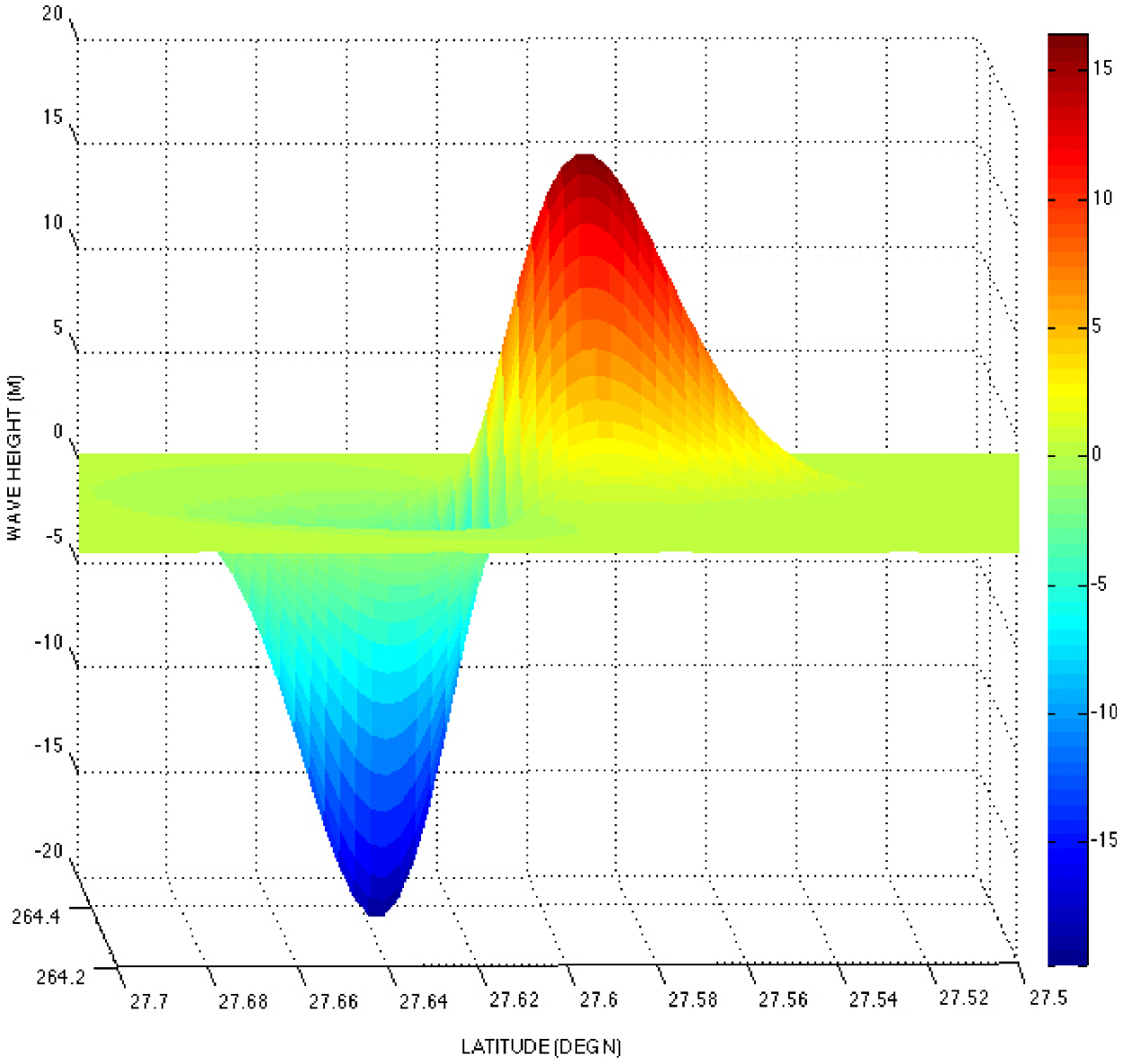

Figure 2.4S.6-12 Plan view of Papua New Guinea (PNG) initial deformation condition. Maximum elevation of negative wave is -18 m (MSL); maximum elevation of positive wave is +16 m (MSL).

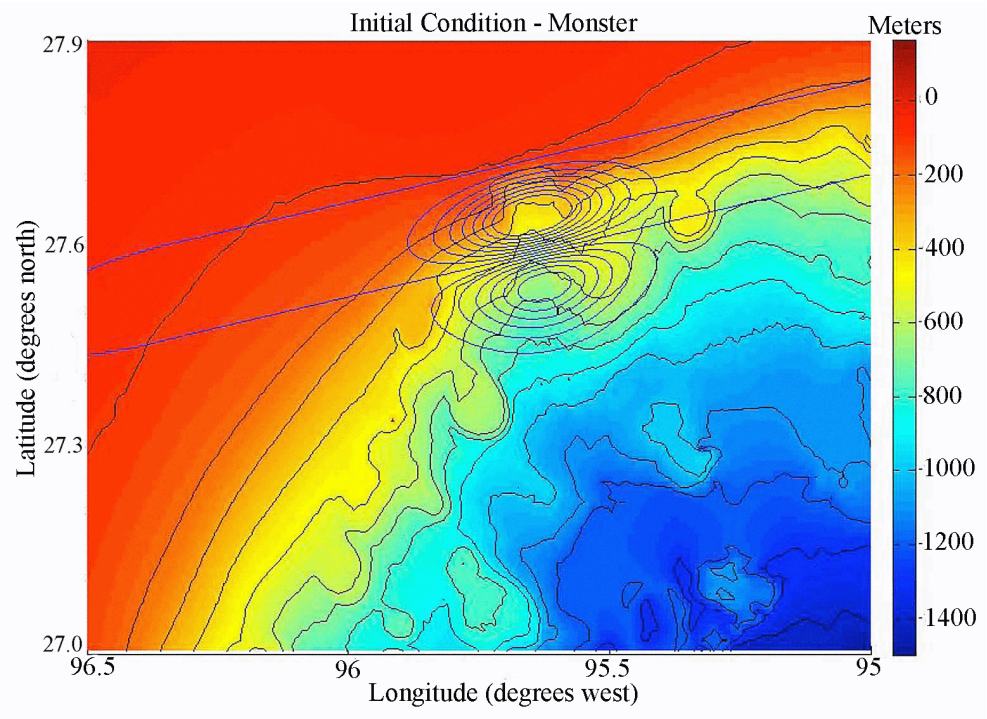

Figure 2.4S.6-13 Plan view of hypothetical "Monster" initial deformation condition at location of the East Breaks slump in the Gulf of Mexico. Elevations of initial wave correspond with elevations in Figure 2.4S.6-14.

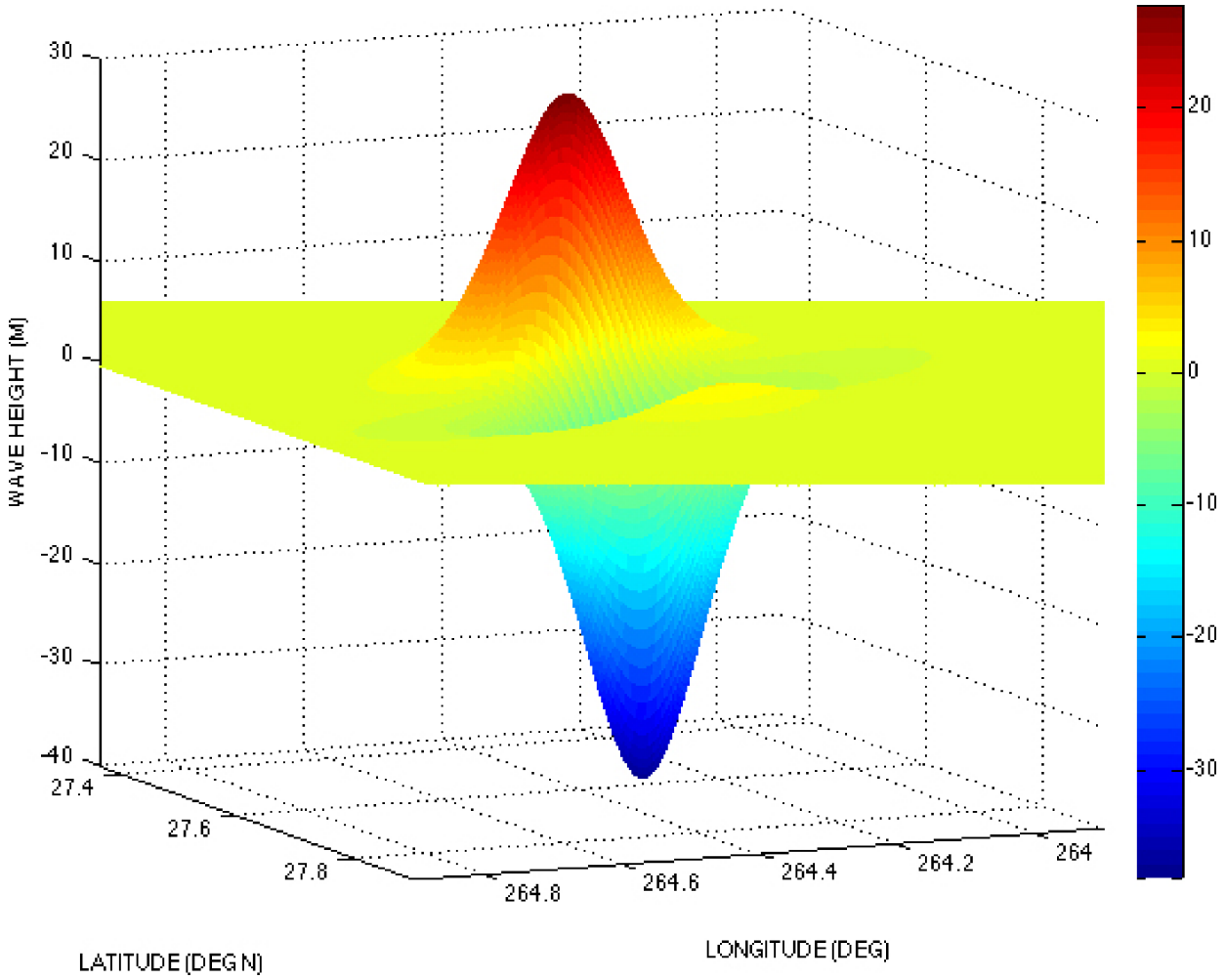

Figure 2.4S.6-14 Oblique view of hypothetical "Monster" initial deformation condition. Maximum elevation of negative wave is -38 m (MSL); maximum elevation of positive wave is +28 m (MSL).

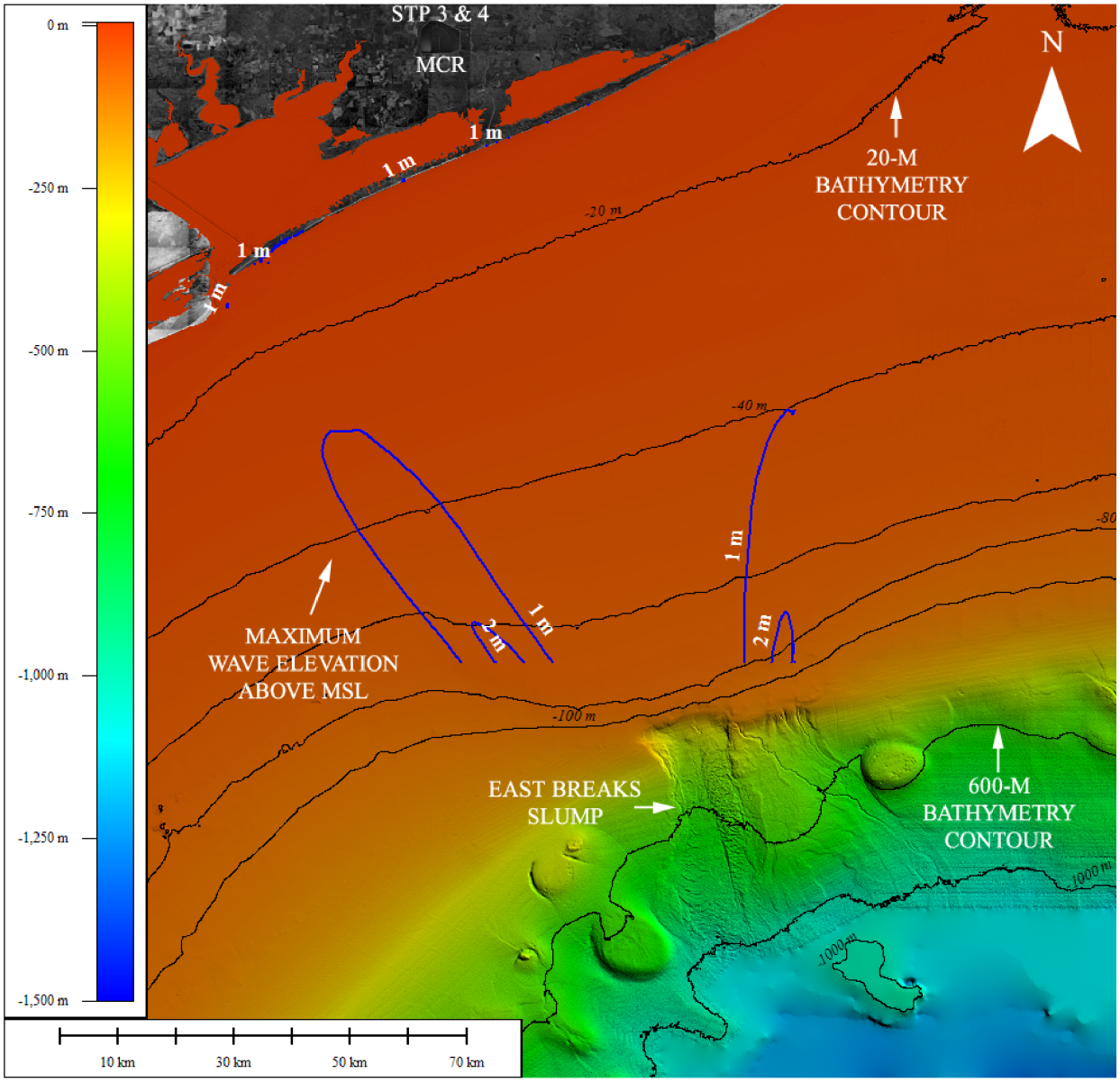

Figure 2.4S.6-15 Maximum coastal runup for the PV simulation was 1 m.

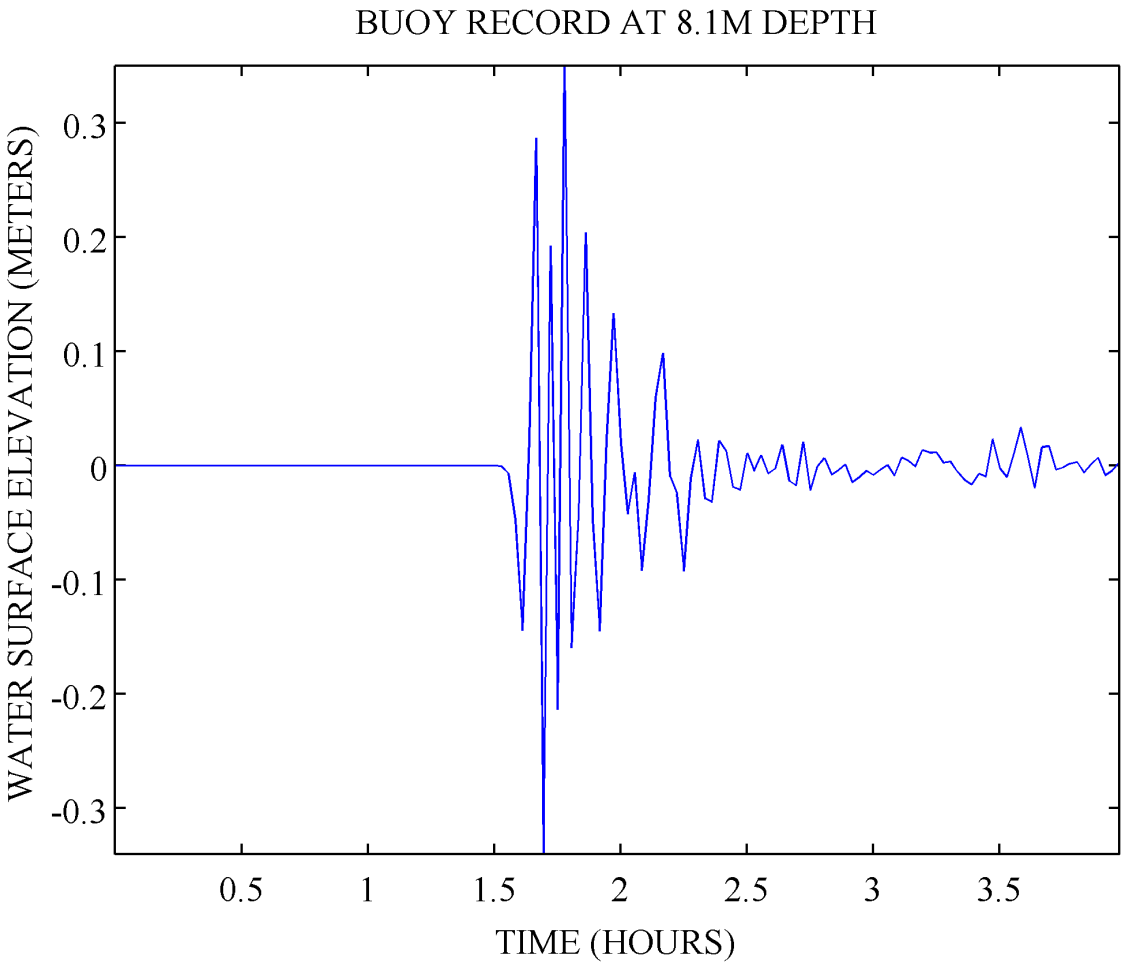

Figure 2.4S.6-16 Time series of wave amplitude for PV simulation at 28.58° N and 95.98° W (i.e., buoy location shown in Figure 2.4S.6-4). Datum referenced to MSL.

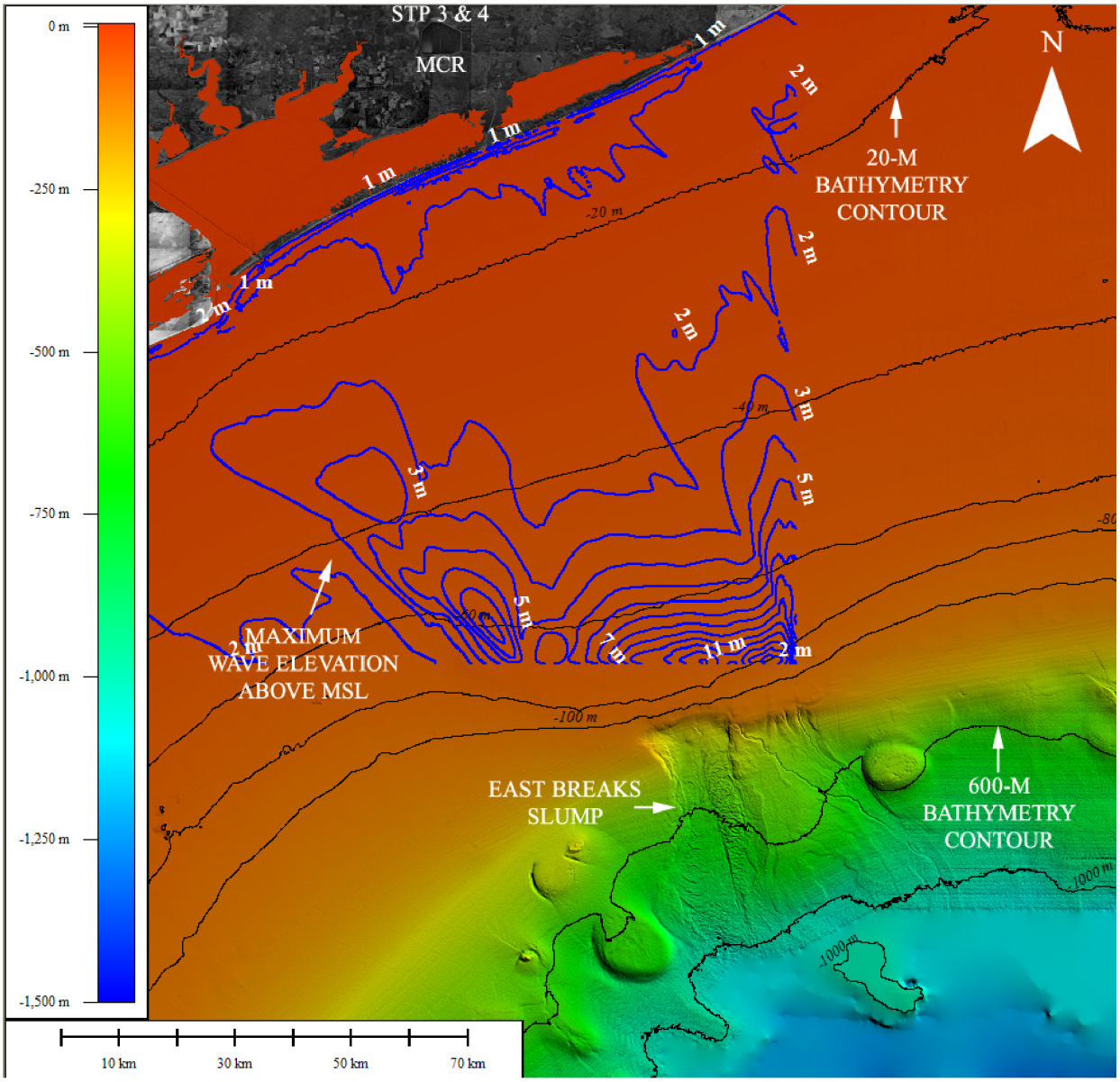

Figure 2.4S.6-17 Maximum coastal runup for the PVx20 simulation was 2 m.

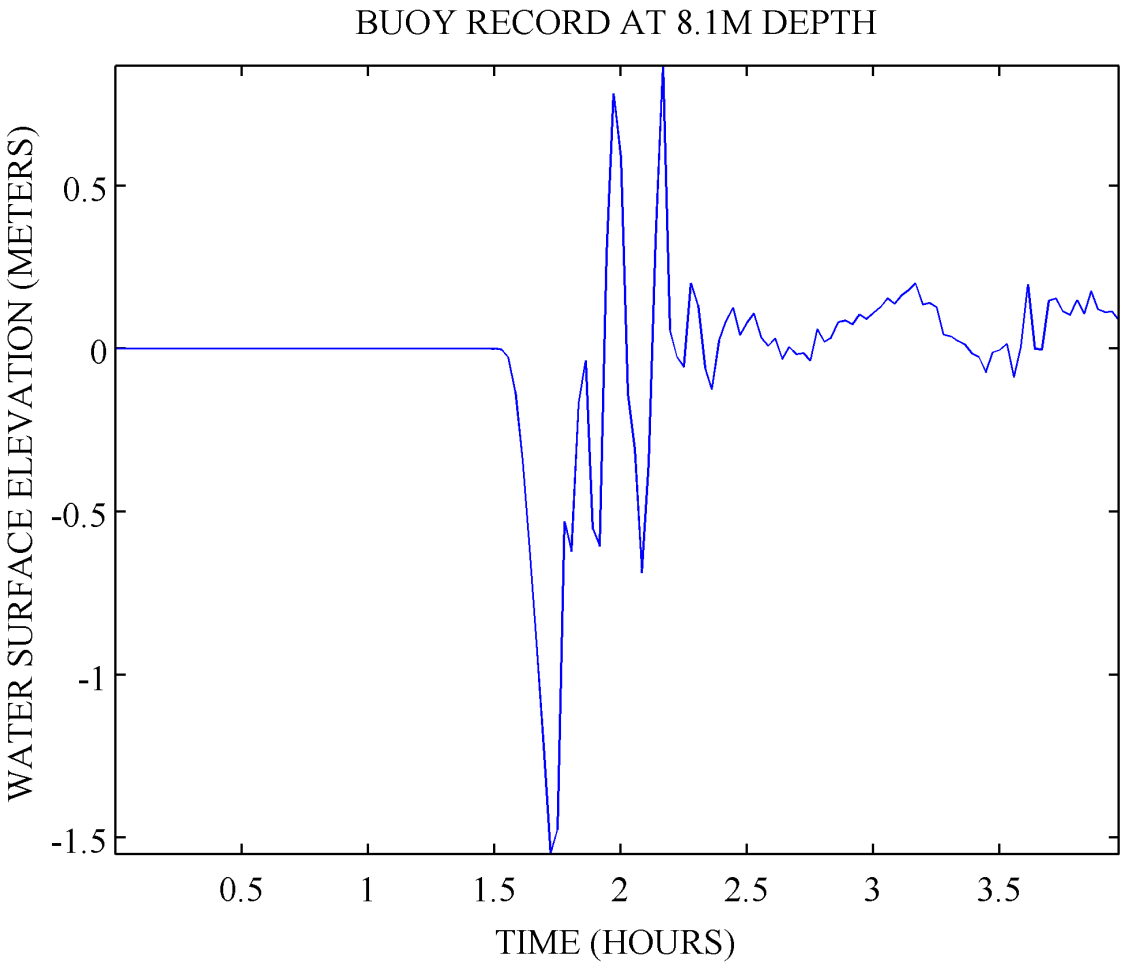

Figure 2.4S.6-18 Time series of wave amplitude for PVx20 simulation at 28.58° N and 95.98° W (i.e., buoy location shown in Figure 2.4S.6-4). Datum referenced to MSL.

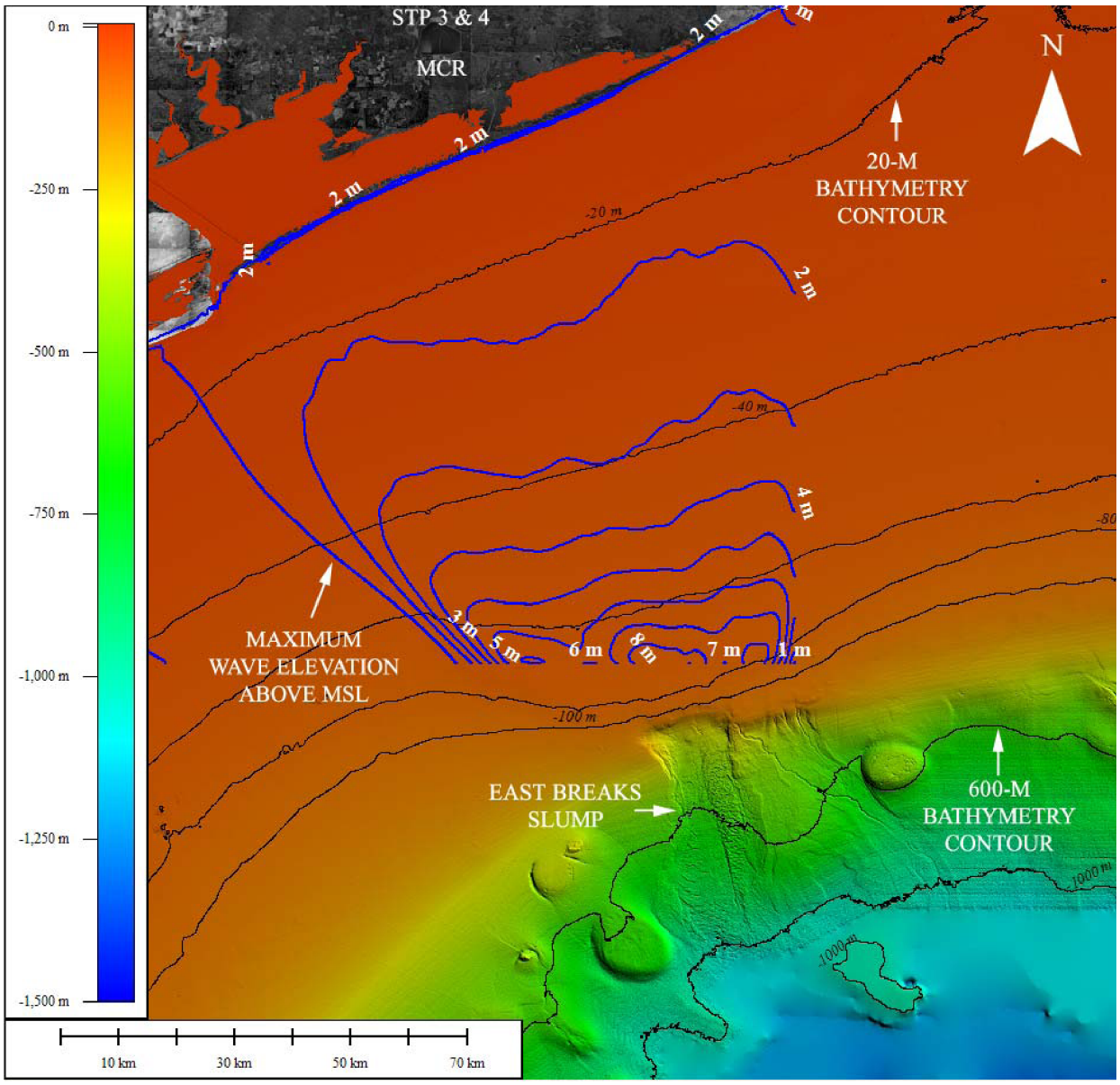

Figure 2.4S.6-19 Maximum coastal runup for the PNG simulation was 2 m.

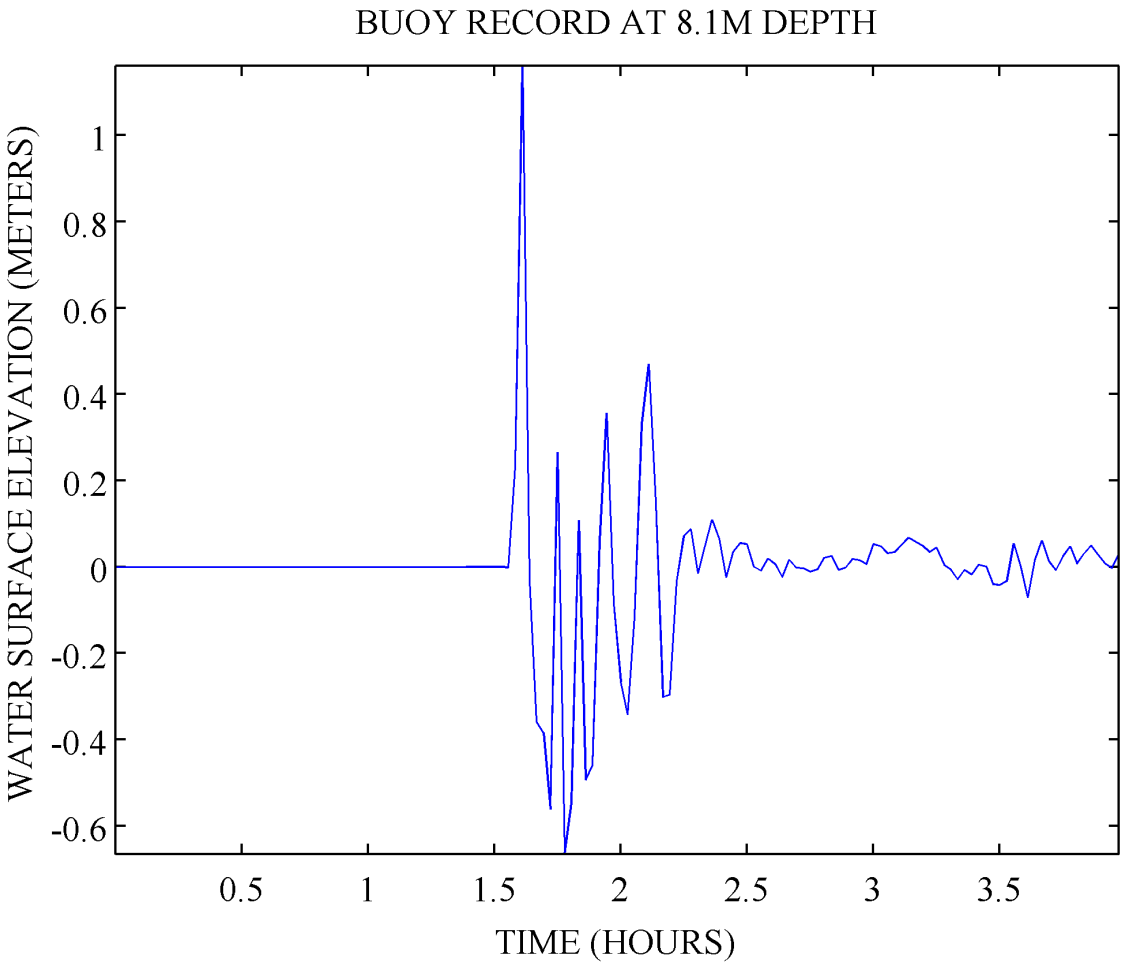

Figure 2.4S.6-20 Time series of wave amplitude for PNG simulation at 28.58° N and 95.98° W (i.e., buoy location shown in Figure 2.4S.6-4). Datum referenced to MSL.

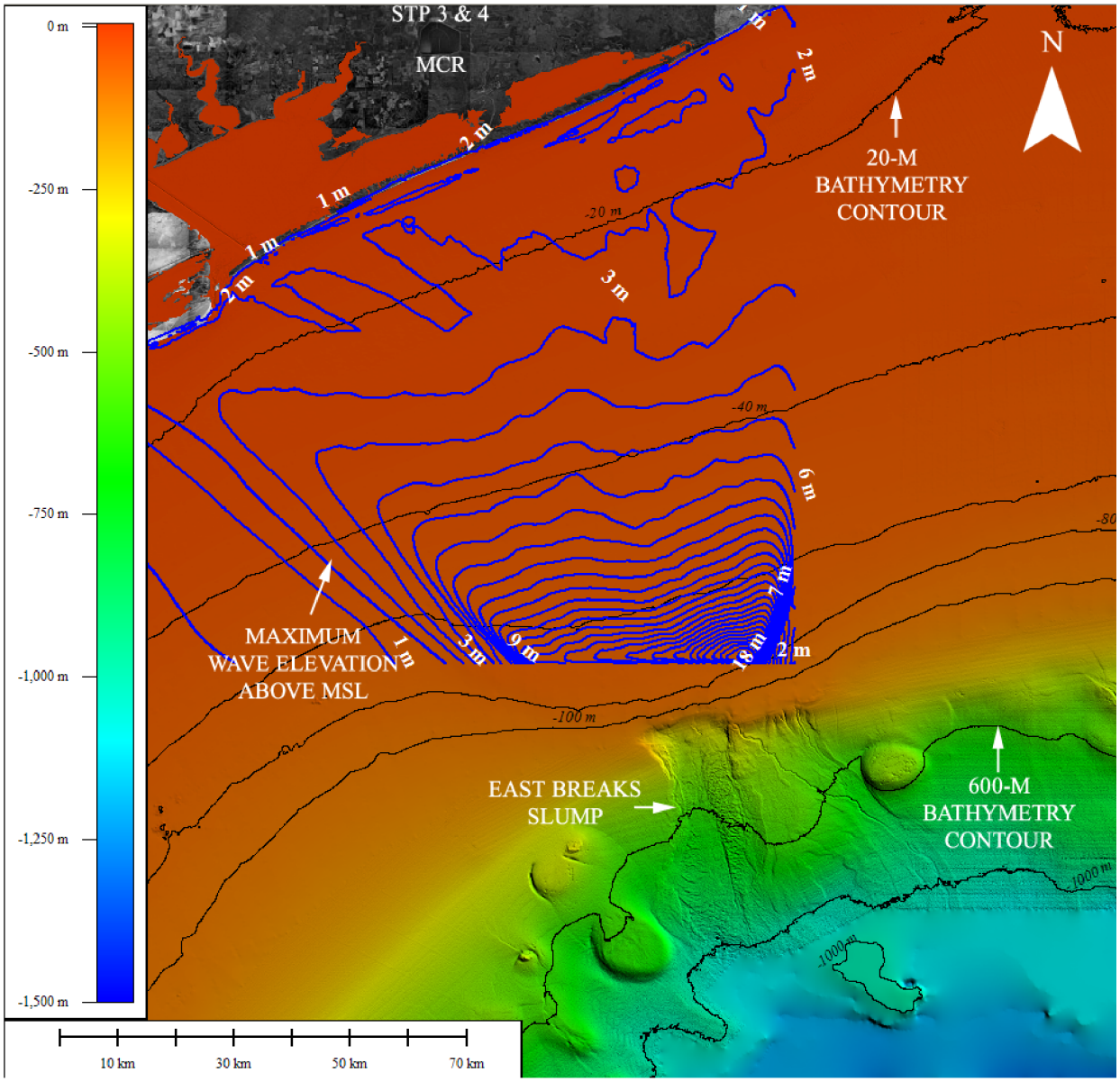

Figure 2.4S.6-21 Maximum coastal runup for the hypothetical "Monster" simulation was 2 m.

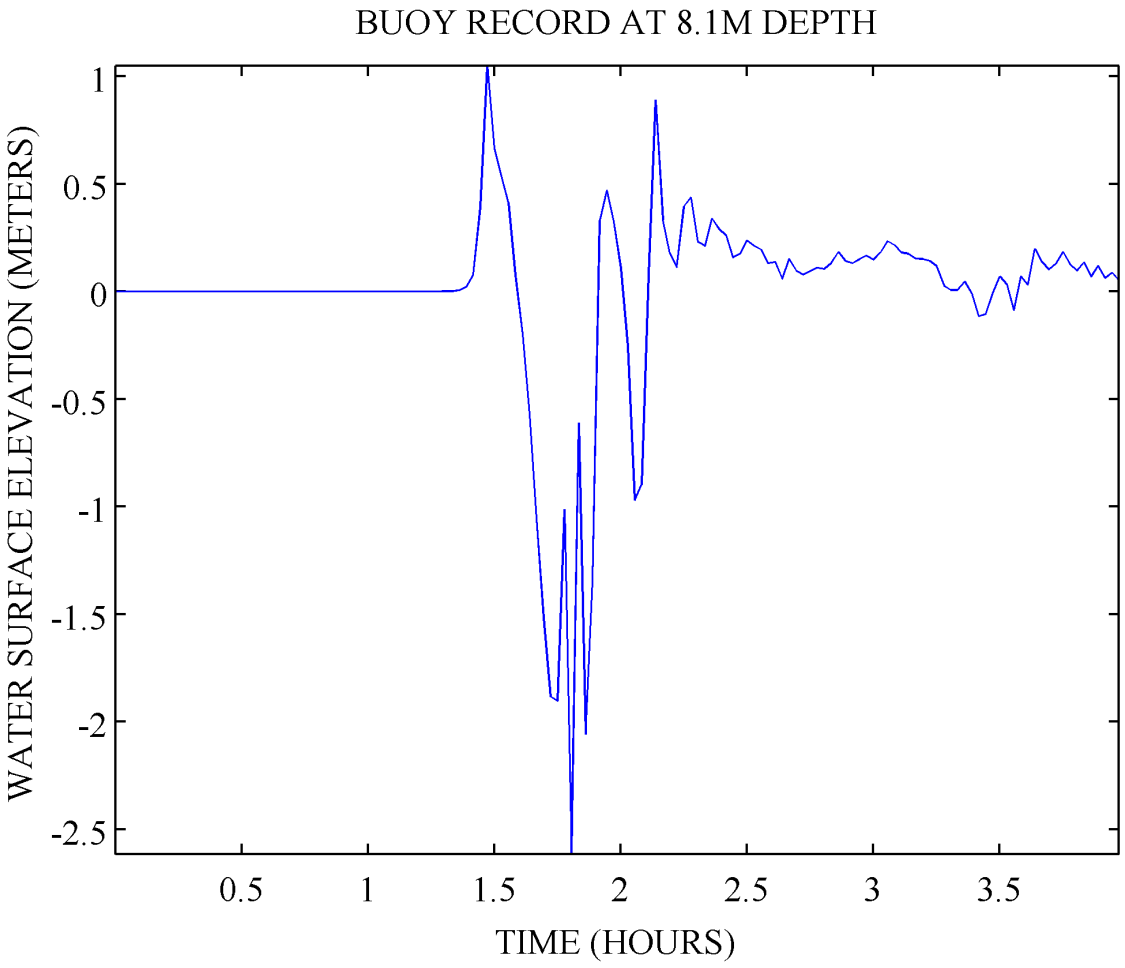

Figure 2.4S.6-22 Time series of wave amplitude for hypothetical "Monster" simulation at 28.58° N and 95.98° W (i.e., buoy location shown in Figure 2.4S.6-4). Datum referenced to MSL.